

Simulation of a 6/4 Switched Reluctance Motor

Based on Matlab/Simulink Environment

F. Soares and P.J. Costa Branco

Laboratório de Mecatrónica, Instituto Superior Técnico
Av. Rovisco Pais, 1049-01, Lisboa Codex, Fax N° 351-21-8417167
E-mail: pbranco@alfa.ist.utl.pt
Portugal

ABSTRACT

This paper describes a Matlab/Simulink environment to simulate a 6/4-switched reluctance motor. From its linear model to the non-linear model, its dynamics is described and discussed in detail. All simulations are completely documented through the paper by their block diagrams and corresponding special Matlab functions and parameters to the reader quickly develop its model. Based on the developed model, simulation studies are performed and compared to measured motor phase currents either for hysteresis and voltage control strategies, and the steady-state motor operation to validate the model.

I. INTRODUCTION

Profits that one can have with a simulation analysis taking account the complete modeling of a system is not anymore to prove today. Indeed, the simulation of a system is important in view of its design and experimental realization [11].

Most studies concerning dynamic simulation of switched reluctance machines (SRM) [3] have been achieved from the programming, either in C language, Fortran, and also employing differential equation-based languages as ACSL [15,16,17]. Even software designed to simulate electric network systems as the EMTDC and EMTP have been used. These techniques, although very useful, they have lack of flexibility if new elements want to be brought, causing the increase of cost with supplementary programming effort. On the other hand, very few simulation studies of the SR machine have been achieved with circuit-based languages as Spice, Simulink, Matrix, Tutsim, Vissim, and even Mathcad. The first simulations appeared have been made thanks to the software Spice [13]. Unfortunately, this technique is not “elegant” because Spice is especially adapted to electronic circuit simulation [14]. Lately, there were some considerable progresses in simulation software as Matlab/Simulink, which allowed to achieve a high flexible modeling environment to electrical machinery, as well shown in a recent book [18], and in particular for SRMs as first shown in [6]. The main benefits to be achieved are:

- gain of time for the simulation development;
- choice of several techniques of numeric resolution;
- and several available libraries for different domains as, for example, fuzzy-logic control, neural networks, and signal processing.

In this paper, the switched reluctance motor is studied using a Matlab/Simulink environment. All simulations are completely documented by their block diagrams, corresponding special Matlab functions and parameters. Section II starts introducing the main characteristics of the switched reluctance machine. Its advantages and disadvantages are indicated and compared with the AC motors. The electromagnetic equations are also presented as well as its process of torque

production.

In Section III, the SRM linear model is first elaborated and used in the Matlab/Simulink simulation of a 6/4 SR machine. The two most frequent SRM energizing strategies, voltage and hysteresis current control, are discussed and illustrated.

The SRM non-linear model is presented in Section IV. By a previous finite element study of our 6/4 SR machine, we obtained its magnetic characteristic, describing in detail its Matlab/Simulink model. An extensive set of simulations is then presented; showing the differences when compared with those obtained with the linear model, being this point more detailed in [10].

Completing the electrical machine analysis, Section V shows experimental results included to validate the machine model.

II. SRM CHARACTERISTICS

In a switched reluctance machine, only the stator presents windings, while the rotor is made of steel laminations without conductors or permanent magnets. This very simple structure greatly reduces its cost. Motivated by this mechanical simplicity together with the recent advances in the power electronics components, much research has been developed in the last decade. The SR machine, when compared with the AC and DC machines, shows two main advantages:

- it is a very reliable machine since each phase is largely independent physically, magnetically, and electrically from the other machine phases, and;
- it can achieve very high speeds (20000 - 50000 r.p.m.) because of the lack of conductors or magnets on the rotor;

However, the SR machine has some limitations:

- it must always be electronically commutated and thus cannot run directly from a DC bus or an AC line;
- its salient structure causes strong non-linear magnetic characteristics, complicating its analysis and control, and;

- the SRM shows strong torque ripple and noisy effects [8,9];

The switched reluctance machine motion is produced because of the variable reluctance in the air gap between the rotor and the stator. When a stator winding is energized, producing a single magnetic field, reluctance torque is produced by the tendency of the rotor to move to its minimum reluctance position. When a rotor pole is aligned with a stator pole, as shown in Fig. 1, there is no torque because field lines are orthogonal to the surfaces (considering a small gap). In this position, the inductance is maximal since reluctance is minimum (one neglects the reluctance of the magnetic circuit). If one displaces the rotor of its position, there will be torque production that will tend to bring back the rotor toward the aligned position.

If current is injected in the phase when in the unaligned position, as shown in Fig. 2, there will not be torque production (or very little). If one displaces the rotor of the unaligned position, then a torque tends to displace the rotor toward the next aligned position.

A. Electromagnetic equations

The instantaneous voltage across the terminals of a phase of an SR motor winding is related to the flux linked in the winding by Faraday's law as

$$V = RI + \frac{d\Psi}{dt}, \quad (1)$$

where V is the terminal voltage, I is the phase current, R is the phase winding resistance, and Ψ is the flux linked by the winding. Because of the double salience construction of the SR motor and the magnetic saturation effects, the flux linked in an SRM phase varies as a function of rotor position θ and the phase current. Equation (1) can be expanded as

$$V = RI + \frac{\partial\Psi}{\partial I} \frac{dI}{dt} + \frac{\partial\Psi}{\partial\theta} \frac{d\theta}{dt} \quad (2)$$

where $\frac{\partial\Psi}{\partial I}$ is defined as $L(\theta, I)$, the instantaneous inductance, and term $\frac{\partial\Psi}{\partial\theta} \frac{d\theta}{dt}$ is the instantaneous

back e.m.f.

B. Torque Production

The SRM can be described by a convex function that only depends on rotor position θ and currents in the n phases $I = (I_1, I_2, \dots, I_n)^t$. This function is the co-energy $\bar{W}(I, \theta)$. In a similar manner, the function energy $W(\Psi, \theta)$, whose variables are the fluxes of n phases $\Psi = (\psi_1, \psi_2, \dots, \psi_n)^t$ and the rotor position, also permits to describe the SRM. Whatever are the vectors Ψ and I , the functions of co-energy and energy, verify the following inequality:

$$\bar{W}(I, \theta) + W(\Psi, \theta) \geq \Psi^t I \quad (3)$$

Thanks to its double saliency, the SRM can have a variation of the magnetic energy and therefore torque production. The partial derivative of the energy function in relation to the rotor position gives the machine torque Γ :

$$\Gamma(\Psi_1, \dots, \Psi_n, \theta) = \frac{\partial W}{\partial \theta}(\Psi_1, \dots, \Psi_n, \theta). \quad (4)$$

Applying this relation to the 6/4 SRM, one has

$$\Gamma(\Psi_1, \Psi_2, \Psi_3, \theta) = \frac{\partial W}{\partial \theta}(\Psi_1, \Psi_2, \Psi_3, \theta). \quad (5)$$

When one energizes one phase, the torque appears so that the rotor evolves in the direction where the inductance increases. Therefore, the torque will be in direction of the nearest aligned position.

III. SRM LINEAR MODEL

The parameters used to simulate the 6/4 SR motor were previously obtained by a finite element analysis in [1]. Fig. 3 shows its linear inductance profile $L(\theta)$ with each phase inductance displaced by an angle θ_s given by

$$\theta_s = 2\pi \left(\frac{1}{N_r} - \frac{1}{N_s} \right), \quad (6)$$

where N_r and N_s are the number of rotor and stator poles, respectively.

When the motor has equal rotor and stator pole arcs, $\beta_r = \beta_s$, one has the following angle relations

$$\theta_x = \left(\frac{\pi}{N_r} - \beta_r \right), \quad (7)$$

$$\theta_y = \frac{\pi}{N_r}, \quad (8)$$

which are indicated in Fig. 3. Fig. 4 shows the angle δ corresponding to the displacement of a phase in relation to another, and given by

$$\delta = 2\pi \left(\frac{1}{N_r} - \frac{1}{N_s} \right). \quad (9)$$

The 6/4 SRM has the following parameters: $L_{min} = 8 \text{ mH}$, $L_{max} = 60 \text{ mH}$, and $\beta_r = \beta_s = 30^\circ$.

Thus, from (7) and (8), one gets $\theta_x = 15^\circ$ and $\theta_y = 45^\circ$.

The electric equation of each phase is given by

$$\frac{d\Psi_i(\theta, I_i)}{dt} + RI_i = V \quad \text{with } i = \{1, 2, 3\}. \quad (10)$$

While excluding saturation and mutual inductance effects, the flux in each phase is given by the linear equation

$$\Psi_i(\theta, I_i) = L(\theta)I_i. \quad (11)$$

The total energy associated with the three phases ($n = 3$) is given by

$$W_{total} = \frac{1}{2} \sum_{i=1}^3 L(\theta + (n-i-1)\theta_s) I_i^2, \quad (12)$$

and the motor total torque by

$$\Gamma = \frac{1}{2} \sum_{i=1}^3 \frac{dL(\theta + (n-i-1)\theta_s)}{d\theta} I_i^2. \quad (13)$$

The mechanical equations are

$$J \frac{d\omega}{dt} = \Gamma - \Gamma_l - f\omega, \quad (14)$$

and

$$\frac{d\theta}{dt} = \omega, \quad (15)$$

where Γ_l represents the torque load, and f the machine friction coefficient.

We show in Fig. 5 the simulation diagram used for the SRM linear model. One can note a strong aspect of the SRM simulation using Simulink that is the use of conventional blocks allowing understanding the programmer's structure more easily. To be more complete, the block named *phase1* is described with details at follow.

Fig. 6 shows the content of block *phase 1*. It contains four other blocks, each one associated with a specific *Matlab* function. They are:

1) *Switch*: permits to assure the power converter commutations at angles θ_{on} , θ_{off} and θ_d .

Appendix III lists the respective Matlab program with associated commentaries.

2) *Inductance*: computes the current on the respective phase inductance according to rotor position θ and phase flux Ψ . Therefore, one gets phase current I as its output signal, as shown in Fig. 6 by output block 3 named *current1*. In Appendix IV, one also lists the respective program.

3) *Torque*: computes the torque produced in this phase according to the rotor position θ and the current value I . In Appendix V, one finds the respective program.

4) *Modulo $\pi/2$* : Each phase inductance has a periodicity of $2\pi/N_r$ degrees. Therefore, it is appropriate to transform the rotor position angle coming from the mechanical equation so that it is modulo $2\pi/N_r$. In Fig. 6, block *modulo $\pi/2$* achieves this function. As to take account of separating angle θ_s , every phase block in Fig. 5 will only differ concerning this point.

Put aside those four Matlab functions, everything concerning the initialization of simulation parameters is located in a file named *int.m*, which is listed in Appendix I. This file permits us to take account of a general model for the 6/4 SRM, meaning that the user will be able to enter other

values than those utilized in this simulation without changing anything in all remaining parts.

To compute each phase electric equation (10), we avoid the derivative action. The simulation diagram in Fig. 6 shows how this was achieved by using a block integrator (1/s) with saturation. This is important because it is necessary that the phase flux does not become negative since the converter is unidirectional in operation. If a pure integrator had been used, followed by a saturating block, it would not have the same effect. Indeed, when the saturating block fixes the output variable to its maximum value, it does not prevent the block integrator to stop the integration, which would introduce a false time delay in the SRM simulation results.

To begin the SRM simulation using its linear model, it is necessary to take care of choosing an initial rotor position that was not in the zone where inductance L had a constant value, since there would not be torque produced. When the load torque is zero, variable θ corresponding to rotor position would not evolve and the machine will be halted all the time. However, when the load torque is not zero, the rotor position will displace to establish a rotor speed where $T_e = T_L$. For our particular machine, an initial θ superior to 15° was chosen, as we can verify in its inductance profile in Fig. 3, in order to avoid the first case of zero torque load.

A. SRM Energizing Strategies

There are several possible configurations to energize a switched reluctance machine from a converter. A good summary can be found in [2]. The different energizing structures distinguish themselves by their number of semiconductors and passive components. They also depend on the number of phases and the way of which the stator coils are connected. The maximum control and flexibility is obtained, however, with the H -bridge asymmetric type converter shown in Fig. 7. Each phase has two IGBTs and two diodes. The number of semiconductors is the same that for an inverter of a synchronous machine. However, the structure is completely different. One can also notice that it is not possible to short-circuit the source because the resistance of the coils limits the current.

Since we stand in linear regime, the flux relation is given by

$$\Psi = L(\theta)I . \quad (16)$$

The co-energy stays

$$\bar{W} = \frac{1}{2}L(\theta)I^2 , \quad (17)$$

resulting in a torque given by

$$\Gamma = \frac{1}{2} \frac{dL}{d\theta} I^2 . \quad (18)$$

Expression (18) shows that this converter is unidirectional in current because torque production does not depend on the current sign but only of $\frac{dL}{d\theta}$ sign.

Follow, we show the two most used energizing strategies for a switched reluctance machine: voltage source and hysteresis current control.

1) *Strategy - Voltage source*: Supposing an ideal inductance shape, simulation curves in Fig. 8 illustrates when the SRM is energized by a voltage source. The control takes place applying the voltage source to a phase coil at turn-on angle θ_{on} until a turn-off angle θ_{off} . After that, the applied voltage is reversed until a certain demagnetizing angle θ_d , which must to allow the return of the magnetic flux toward zero.

To apply voltage V in one phase, the two IGBTs Q1 and Q2 in Fig. 7 must be ON. On the contrary, to apply the $-V$ voltage and assure the current continuity, the two diodes D1 and D2 are used.

Follow, we verify in more detail the phase energizing. From the phase voltage relation

$$V = RI + \frac{d\Psi}{dt} \quad (19)$$

with $\Psi = L(\theta)I$, one has

$$d\Psi = \frac{\partial\Psi}{\partial\theta}d\theta + \frac{\partial\Psi}{\partial I}dI , \quad (20)$$

and

$$\frac{d\Psi}{dt} = I \frac{dL}{d\theta} \omega + L(\theta) \frac{dI}{dt}, \quad (21)$$

resulting in

$$V = RI + L(\theta) \frac{dI}{dt} + I\omega \frac{dL}{d\theta}. \quad (22)$$

In equation (22), term $I\omega \frac{dL}{d\theta}$ is the f.e.m induced voltage, which will be high for high speeds. To increase the current growth and avoid a high f.e.m opposition, the θ_{on} angle must be chosen in the same way as in Fig. 8, which means chosen when both inductance and the f.e.m are minimum.

Using the linear model, the minimum f.e.m value will be zero since $\frac{dL}{d\theta} = 0$, as shown in Fig. 8(d).

However, when the rotor position is in the zone where the inductance increases, the f.e.m voltage appears. After, when the f.e.m. surpasses voltage V , phase current starts to decrease until angle θ_{off} is reached, as shown in Fig. 8 (c).

The sharp switching effects present in the voltage energizing strategy clearly introduces harmonics in the torque signal, by phase current signal, that increase the motor speed ripple. Since this energized strategy is usually applied only when the motor had reached high speed values, the mechanical system will attenuate these harmonics from the motor speed signal.

To illustrate the importance of choosing an adequate θ_{off} angle, we have set a higher θ_{off} value for results of Fig. 9. In Fig 9(c), we can observe that phase current does not reach a zero value anymore. Still, one can see in zone 1 that current starts decreasing less quickly because now we are in the decreasing region of the inductance, which did not happen before in Fig. 8(c). When in zone 2, the f.e.m becomes significant again (see Fig. 9 (d)) since the phase voltage passes from $-150V$ to $0V$ and so phase current starts increasing. At last, in zone 3, phase current starts decreasing because the f.e.m. voltage is again null since the inductance is constant, $\frac{dL}{d\theta} = 0$.

Fig. 10 shows a second set of simulation results using $\theta_{on} = 0^\circ, \theta_{off} = 30^\circ$, and with the

machine functioning without load applied. One notes in Fig. 10 (a) that the θ_{off} angle value is now enough to avoid that the current starts growing when the aligned position is reached. As expected, one can see in Fig. 10 (b) that the phase current produces a very small negative torque. However, the total torque is always positive, as shown in Fig. 10 (d), because the negative torque produced in one phase is compensated by the other torque phases. The motor speed signal presents, however, strong oscillations in permanent regime, as shown in Fig 10 (c), since torque ripple is large.

2) *Hysteresis current control*: Dynamic behavior of the SRM is illustrated follow in a case where the hysteresis current controller is employed. These results, shown in Fig. 11, have been achieved for $\theta_{on} = 0^\circ$, $\theta_{off} = 38^\circ$, and a current reference of $I_{ref} = 8A$, with the motor functioning without load. Fig. 11 (a) shows the influence of the hysteresis current control on the shape of phase current. One notices in this figure by zone 1 that the hysteresis band does not remain constant. During zone 1, the phase inductance remains constant and with its minimum value during 15 degrees. One can also observe in Fig 11 (b) the current control influence on the phase torque. Torque ripple presents high magnitude for the used values of θ_{on} and θ_{off} , as shown in Fig 10 (d), having for consequence to originate some important speed oscillations shown in Fig 10 (c).

To decrease the speed oscillations it is necessary to produce more torque. Therefore, we adjusted the θ_{off} angle value from 30° to 38° . The new SRM dynamics is shown in Fig. 12 achieved for $\theta_{on} = 0^\circ$, $\theta_{off} = 38^\circ$, $I_{ref} = 8A$, and with the machine continuing to operate without load. Fig. 12 (a) presents the current shape in one phase. In Fig. 12 (b), one observe that the new value of θ_{off} makes the phase current still to be present in the region of the decreasing phase inductance with the appearing of a negative torque. Fig 12 (d) shows that torque ripple has decreased after adjusting the turn-off angle, and so the machine speed presents now fewer oscillations as shown in Fig. 12 (c). However, ripple reduction is not an easy task because other parameters as the motor speed and load values come to influence the torque ripple magnitude.

The hysteresis current controller is used for low and middle speeds because one has enough time

to be able to control the phase current (Fig. 13). What also permits to use this current control mode at low and middle speeds, it is the fact that the f.e.m. does not take large values that come to impair the current shape. To illustrate the inefficiency of the hysteresis current control for high speeds, Fig. 14 shows a situation where the hysteresis current control is badly assured due to f.e.m. effects.

B. Remarks

In the hysteresis current control, one can distinguish two methods that allow the current to remain in the hysteresis band: to apply the voltages $+V$ and $-V$ depending on the current error $(I_{ref} - I)$ be positive or negative, or apply voltages V and zero. In the first case, according to the current error, either the IGBTs conduct, either are the diodes conducting. In the second case, Fig. 7 shows that IGBT Q2 is always open during the regulation phase, while Q1 is blocked either opened according to the error.

With regard to the turn-on angle θ_{on} , most authors recommend to anticipate its value to the moment where phase inductance begins to increase, to be able to take advantage of a high di/dt . However, it is proper to notice that if one applies the turn-on angle too early, we will be in a region where the inductance change in relation to the rotor position is small. Therefore, the produced torque will be small ($\tilde{A} = \frac{1}{2} \frac{dL}{d\hat{e}} i^2$). On the other hand, the current will be high, increasing the power losses. Hence, it is necessary to choose an appropriately value to θ_{on} if one wants to optimize the motor efficiency.

IV. SRM NON-LINEAR MODEL

The non-linear character of the SRM magnetic characteristic $B = f(H)$ is now considered. Before presenting its Matlab-Simulink simulations, we overview some methods that allow to model the SRM in its non-linear regime.

Most authors to take account the non-linearity of the SRM magnetic characteristic proposed

analytic solutions. Some among them approximate from experimental data the inductance profile $L(\theta, I)$ of the SRM by trigonometric functions [4], or even using a cubic spline interpolation [12]. In both solutions, the torque is computed by an analytical way using $\Gamma(\theta, I) = \partial \bar{W}(\theta, I) / \partial \theta$. A more complete summary of these methods can be found in [5]. However, these methods pose some problems. They involve extensive calculations, besides they require derivative calculations that accentuate the computational time of SRM simulations. In spite of all, the main defect of these methods resides in the results precision. Take the example of a polynomial interpolation. Indeed, even though polynomial coefficients are computed with a good precision, mistakes on flux derivative $\partial \Psi(\theta, I) / \partial \theta$ can be important, as shown in [5].

The key to achieve a good simulation of a switched reluctance machine is to use a methodology that permits to take account the non-linearity of its magnetic characteristic while minimizing the simulation time. The procedure that we used with Matlab-Simulink consisted in avoiding all partial derivatives because those would be source of errors. The technique was to utilize a look-up table which approximates the relations flux/current/position and current/torque/position, as demonstrated in [6] and [7].

In a previous paper [1], our 6/4 SR machine was modeled by a finite element analysis (FEM) providing us with its different magnetic data for the realization of the look-up tables. These data was provided under a matrix shape of size 966 lines and 6 columns, with each column corresponding to the rotor position, phase current, flux, torque produced in the phase, the inductance values, and the mutual fluxes. Using these data, the look-up tables were achieved for 46 rotor positions from 0° to $+45^\circ$, and 21 different current values from 0 to 20A.

A. Inductance profile and magnetic characteristic

The inductance profile $L(\theta, I)$ obtained from the FEM analysis is displayed in Fig. 15 for different values of phase current and rotor position. The inductance is minimum when the rotor and stator are in unaligned position. On the other hand, it reaches its maximum value for the aligned

position, where the saturation regime is reached more easily. The inductance curve is not linear and shows that for large currents there are large saturation effects. Fig. 15 admits two axes of symmetries in $\theta = 0^\circ$ and in $\theta = +45^\circ$, unaligned and aligned positions, respectively. Fig. 16 shows the magnetic flux for different rotor positions and phase currents, revealing the saturation effects. The lowest curve corresponds to the unaligned position and the curve of the top corresponds to the aligned position.

Fig. 17 shows the electromagnetic torque as a function of rotor position and phase current values. The figure shows the influence of the non-linearity of the magnetic characteristic on the phase torque. To achieve this curve, a linear interpolation has been used, which was sufficient because many intermediate points were obtained from the FEM analysis. One also notes in Fig. 17 that while approaching the aligned rotor position the phase torque decreases. This is caused by the saturation effect, which decreases the co-energy variation.

B. Simulation.

Comparing with Simulink scheme of the linear model in Fig. 5, the Simulink structure of the non-linear SRM model did not change. On the other hand, blocks *phase 1*, *phase 2* and *phase 3* becomes different. Fig. 18 shows, for example, the new block *phase 1*. It shows two look-up tables: flux/theta/current (*table current*) and current/theta/torque (*table torque*). These tables were obtained using the block “Look-Up Table” available in the non-linear category of Simulink. The look-up table giving phase current I was achieved by a linear interpolation between the input flux vector Ψ , corresponding to table lines, and the rotor position vector θ that corresponds to the table columns. In Fig. 19, we display the table data that permitted to achieve the look-up tables. Blocks *phase 2* and *phase 3* are similar to *phase 1*.

C. Remark

The most difficulty task is the construction of the look-up tables from the FEM data matrix 966

by 6. Appendix VI lists the Matlab program named *int2.m*, which allowed building the two tables. In Fig. 18 there is a block denoted by *Angles compatibility*. This block refers to a Matlab function that converts angles in radians to degrees. In Appendix II, we also list the program that does this conversion and respective commentaries.

D. Numerical results.

As for the linear model, simulation results have been achieved with voltage control and hysteresis current controller.

Voltage control: Fig. 20 shows the results for $\theta_{on} = 0^\circ$ and $\theta_{off} = 30^\circ$, with the machine functioning without load. The considerable difference between the results with the linear model and these, with the non-linear model, is the torque signal. In the linear model, since the saturation effect is not taken in account, the machine torque presents large values, as already shown in Fig. 10 (d). On the other hand, the torque magnitude with the non-linear model are less small due to the saturation, as shown in Fig. 20 (d).

Hysteresis current control: Results in Fig. 21 have been achieved for $\theta_{on} = 0^\circ$, $\theta_{off} = 30^\circ$, $I_{ref} = 10A$, and without torque load. In relation to the results previously shown in Fig. 11 with the linear regime, the differences between the two models for the case of an hysteresis current control is not as impressive as was for the voltage control case. However, comparing torque signal in Fig 11 (d) obtained with the linear model, with the one in Fig. 21 (d) from the non-linear model, the torque rate reveals the saturation effects. In spite of all, one verifies that torque ripple are again significant, which indicates that the value of 30 degrees set to θ_{off} angle is inadequate for the current machine operating point. Fig. 21(c) also shows that this choice of θ_{off} makes the speed ripple to be high.

The second set of results described in Fig. 22 were obtained with the turn-off angle increased from 30° to a value of $\theta_{off} = 40^\circ$. Fig. 22 (d) reveals that torque ripple has decreased. However, one notices in Fig. 22 (b) that each phase produces now more negative torque because of the new turn-off angle value. Consequently, phase current is still present when the aligned position is reached, as indicated in Fig. 22 (a). In spite of all, this operating point proves by Fig. 22 (c) and 22 (d) to be better for a torque and speed ripple reduction. Note that the negative torque produced by one phase did not have an impact on the total torque since it is compensated by the other torque signals generated in the other two phases.

To have a better general view of the influence of I_{ref} and θ_{off} values in the mean torque Γ_{mean} and their influence in the torque oscillations by the variance signal σ , Fig. 23 displays first the functional relation of the mean torque $\Gamma_{mean} = g(I_{ref}, \theta_{off})$. In Fig 24, we plot the torque variance signal as function of I_{ref} and θ_{off} , $\sigma = f(I_{ref}, \theta_{off})$. One notices that for different values of reference current, there is always a θ_{off} value that maximizes the mean torque (see Fig. 23), as well minimizes the variance and so torque oscillations (see Fig 24).

V. EXPERIMENTAL RESULTS

In this section, simulation and experimental results are presented and compared for model validation. A switched reluctance drive prototype was used, consisting of the 6/4 SR machine and a H-bridge power converter. The electrical machine, constructed based on the finite element study of [1] and whose magnetic data was used in our simulation model, is shown in Fig. 25.

The H-bridge power converter is shown in Fig. 26. As indicated in the figure, the converter uses IGBTs with freewheeling diodes, and the continuous voltage V_d is obtained from a diode rectifier. The power converter was implemented limiting each phase current to 5A. This was effectuated because the objective was to operate the machine in the corner of the magnetic characteristics where the machine efficiency is near its maximum. That stator current limitation has restricted, however,

our validation tests to current values that not saturate the machine. Despite this, the model is suitable to the normal operation of the SR motor as the next validation tests show.

An hysteresis current controller is used with the microcomputer establishing the energizing and reenergizing angles, and the reference current signal.

With the prototype, tests could be initiated to verify the developed SRM model. They were effectuated with the SR drive system operating in open-loop mode and for a set of different operating conditions.

Fig. 27(a) shows the SR motor phase current measured when the machine operates for a current reference of 2A, nominal DC voltage, using the θ_{on} and θ_{off} parameters listed in Table I. In Fig. 51(b) the same operating conditions has been simulated using the developed model and same sampling time. A close correlation of simulated with experimental currents can be observed.

In Fig. 28 (a) and (b) the experimental and simulated results are shown when the drive operates with a lower DC voltage ($V_d = 100$ V). The other operating parameters remained the same, as shown in Table I.

In the previous tests, the hysteresis current controller was considered. For a voltage control test, the motor operated with 30V of DC voltage, using the parameters listed in Table II. By comparing the experimental measured current shown in Fig. 29(a) with the simulated waveform in Fig. 29(b), it is seen that the waveforms are almost identical.

A commonly applied procedure that can be considered as a test of the model validity for simulation is to compare measured and simulated steady-state characteristics. For comparison of the motor steady-state operation obtained with the model and the experimental prototype, two tests were effectuated. These considered two reference current values, $I_{ref} = 1.5$ A and $I_{ref} = 2.5$ A, and variation of the θ_{off} angle from 40 to 67 degrees. Fig. 30(a) and (b) show the measured and simulated motor speed obtained for 1.5 A and 2.5 A, respectively. From the figures, it is seen that the steady-state responses of the model matches the measured data well.

VI. CONCLUSION

This paper has described and discussed in detail how from Matlab-Simulink one can achieve the simulation environment for a switched reluctance motor. We verified that to analyze with precision the torque oscillations of a SRM, a simulation study using its linear model is not appropriate. Several simulations have been achieved in order to study the dynamic behavior of the SRM. We mainly verified the influence of the turn-off angle θ_{off} in its dynamic behavior. It was proved dependent of the machine's operating point and that exists a θ_{off} value, which allow torque ripple reduction.

For model validation, phase current either for hysteresis and voltage control strategies, and the steady-state systems operation data were measured and compared to the estimated model responses. The validation study indicated that using the developed model, enough accurate results can be obtained with it.

ACKNOWLEDGEMENTS

The authors would like to thank the anonymous referees for many helpful comments and suggestions aimed at improving and clarifying the original manuscript of this paper.

REFERENCES

- [1] J. Nascimento, L. Rolim, P. Heidrich et al, "Design and simulation aspects of a switched reluctance drive", *Proc. of 4^o Brazilian Power Electronics Conference (COBEP96)*, pp. 79-83, São Paulo, 1996.
- [2] T.J.E Miller, *Switched reluctance motors and their control*, Oxford, Magma Physics Publishing and Clarendon Press-Oxford, 1993.
- [3] P.J. Lawrenson, J.M. Stephenson, P.T. Blenkinsop, J. Corda and N.N. Fulton, "Variable-speed switched reluctance motor", *IEE Proceedings Inst. Elect. Eng.*, Vol. 127, no. 4, pp. 253-265, June 1980.
- [4] H. Henao, G.A. Capolino, E. Bassily and M. Poloujadoff "A new control angle strategy for switched reluctance motor", *Proc. of EPE'97*, Vol. 3, pp. 613-618, 1997.
- [5] J.M Stephenson et J. Corda, "Computation torque and current in doubly salient reluctance motors from nonlinear magnetization data", *IEE Proc.*, Vol. 126, no. 5, pp. 393-396, May 1979.
- [6] C.R. Elliot, J.M. Stephenson et M.L. McClelland, "Advances in switched reluctance drive system dynamic simulation", *Proc. of EPE'95*, Vol.3, pp. 622-626, 1995.
- [7] M.G. Simões, W.I. Suemitsu, P.J. Costa Branco, J.A. Dente et L.G. Rolim, "Fuzzy logic control for a switched reluctance motor", *IEEE International Symposium on Industrial Electronics (ISIE'97)*, Vol.2, pp. 527-531, June 1997.
- [8] M. Rodrigues, P.J. Costa Branco and W. Suemitsu, "Fuzzy Logic Torque Ripple Reduction by Turn-off Angle Compensation for Switched Reluctance Motors", To appear in *IEEE Trans. on Industrial Electronics*. (Available as a technical report at <http://pbranco.ist.utl.pt>).
- [9] L. Henriques, L. Rolim, W. Suemitsu, P.J. Costa Branco and J.A. Dente, "Torque Ripple Minimization in a Switched Reluctance Drive by Neuro-fuzzy Compensation", To appear in *IEEE Trans. on Magnetics*. (Available as technical report at <http://pbranco.ist.utl.pt>).

- [10] P.J. Costa Branco, "Influence of Magnetic Nonlinearities on Simulation Accuracy of Switched Reluctance Motor Models", In: *Systems and Control: Theory and Applications*, pp. 403-408, World Scientific and Engineering Society Press, Danvers, USA. (Available as technical report at <http://pbranco.ist.utl.pt>)
- [11] B.K. Bose, T.J.E. Miller et P.M. Szczesny, "Microcomputer control of switched reluctance motor", *IEEE Transactions on Industry Applications*, Vol.IA-22, no.4, pp. 708-715, June 1986.
- [12] D.W.J. Pulle et I.R. Petersen, "A generalized approach to torque and current computation", *Proc. of EPE'97*, Vol. 3, pp. 547-551, 1997.
- [13] Franceschini G., Pirani S., Rinaldi M., Tassoni C., "SPICE assisted simulation of controlled electric drives: an application to switched reluctance drives", *IEEE Transactions on Industry Applications*, Vol.IA-27, no.6, pp. 1103-1110, Nov./Dec. 1991.
- [14] O. Ichinokura, T. Onda, M. Kimura, T. Watanabe, T. Yanada and H.J. Guo, "Analysis of Dynamic Characteristics of Switched Reluctance Motor Based on SPICE," *IEEE Transactions on Magnetics*, Vol. 34, No. 4, pp. 2147-2149, 1998.
- [15] Skvarenina, Wasynczuk, Krause, "Simulation of a Switched Reluctance Generator/More Electric Aircraft Power System," *Proc. of 1996 IECEC*, Paper 96398.
- [16] X. Radun, " Switched Reluctance Starter/Generator Modeling Results," *Proc. of SAE Aerospace Atlantic Conference*, Paper 951407, 1995.
- [17] S.D. Pekarek, O. Wasynczuk, H.J. Hegner, "An Efficient and Accurate Model for the Simulation and Analysis of Synchronous Machine/Converter Systems", *IEEE Transactions on Energy Conversion*, pp42-49, March, 1998.
- [18] C-M. Ong, *Dynamic Simulation of Electric Machinery using Matlab/Simulink*, Prentice-Hall, 1998.

APPENDIX I

```

% init.m

% initialization program

% this program allows to change certain parameter values without any change in
% the other Matlab functions

global TETAS TETAX TETAY TETAXY TETAON TETAOFF TETAQ V AUP BUP ADOWN BDOWN DL A
B LMIN LMAX

NS=6                                % number of stator poles
NR=4                                % number of rotor poles
P=3;                                % number of phases
BETAS=30*(pi/180);                  % angle of the rotor pole
BETAR=30*(pi/180);                  % angle of the stator pole
TETAS=(2*pi)*((1/NR)-(1/NS))
TETAX=(pi/NR)-((BETAR+BETAS)/2)
TETAY=(pi/NR)-((BETAR-BETAS)/2)
TETAZ=(BETAR-BETAS)/2
TETAXY=(TETAY+TETAZ+TETAS)
TETAON=20*(pi/180)                  % turn-on commutation angle
TETAOFF=30*(pi/180)                 % turn-off commutation angle
TETAQ=60*(pi/180)                   % angle corresponding to null the phase flux
TETAON=20.1*(pi/180)                 % initial rotor position angle
V=150                                % voltage
R=1.30;                              % phase resistance
J=0.0013;                            % inertial value
F=0.0183;                            % friction coefficient
I=5;                                  % reference current
DELTAI=0.2;                          % hysteresis band
DELTAVMIN=0;
DELTAVMAX=150;
LMIN=8e-3;                            % minimum inductance
LMAX=60e-3;                           % maximum inductance

% program below computes from the giving minimum and maximum inductance
% values, the equations of the linear inductance profile for the increasing
% and decreasing part

G=(inv([TETAX 1;TETAY 1]))*([LMIN;LMAX]);
AUP=G(1);                             % used by the program l.m
BUP=G(2);                             % used by the program l.m
H=(inv([(TETAY+TETAZ) 1;TETAXY 1]))*([LMAX;LMIN]);
ADOWN=H(1);                            % used by the program l.m
BDOWN=H(2);                            % used by the program l.m
DL=AUP;                                % used by the program t.m

% increasing phase inductance: AUP*teta+BUP
% decreasing phase inductance: ADOWN*teta +BDOWN.

```

APPENDIX II

```
% pie.m

% block named "modulo pi/2"

function s=f(e);    % s is the output and e the input variable
s=rem(e,pi/2);     % rem is a Matlab function computing the module operation

%%%%%%%%%%%%%%%%%%%%%%%%%%%%%%%%%%%%%%%%%%%%%%%%%%%%%%%%%%%%%%%%%%%%%%%%

% angle.m

% block named "compatibility of angles"

% this function does the interface between the blocks with angles in radians and
% those in degrees

function y=f(e);

a=(pi/180)*45;
b=(pi/180)*90;

%
if ((e >= 0) & (e <= a))
y=((e*(180/pi))-45);
end;

if ((e > a) & (e <=b))
y=(45-(e*(180/pi)));
end;
```

APPENDIX III

```
% switch.m

% program used for the hysteresis current control
%
% this program allows to chose the commutation instants of the semiconductors
%

function Va=f(TE);      % Va is the output current, TE is the line input
                        % vector
E=TE';                 % E now is the input column vector
e=E(1);                % input current for an hysteresis current control
teta=E(2);             % variable angle modulo pi/2

% the following global command allows to generalize the respective variables to
% other Matlab files;
% variables TETAON and TETAOFF were already defined as global in the
% initialization file int.m;
%

global TETAS TETAX TETAY TETAXY TETAON TETAOFF TETAQ V AUP BUP ADOWN BDOWN DL
LMIN LMAX

if ((TETAON <= teta) & (teta <= TETAOFF))
Va=e;
end;
if ((TETAOFF < teta) & (teta <= TETAQ))
Va=-V;
end;
if (teta >TETAQ)
Va=0;
end;
```

APPENDIX IV

```
% inductance.m

% inductance program (linear model)
% this program gives the output current. The input variables are: flux and teta

function U=f(TE);          % U is the output current variable
                           % TE is the input line vector
E=TE';                    % E is the input column vector
flux=E(1);                % input flux
teta=E(2);                 % input angle modulo pi/2

global TETAS TETAX TETAY TETAXY TETAON TETAOFF TETAQ V AUP BUP ADOWN BDOWN DL
LMIN LMAX

% if the teta value is situated between 0 and TETAX then the output is computed
% as flux/Lmin since during this interval the inductance is constant

if ((0 <= teta) & (teta <= TETAX))
U=[flux/LMIN,LMIN];
end;

% using the values computed in the initialization file int.m, we obtain for this
% interval the value of the current knowing the inductance equation

if ((TETAX < teta) & (teta <= TETAY))
U=[flux/((AUP*teta)+BUP),((AUP*teta)+BUP)];
end;

if ((TETAY < teta) & (teta <= TETAXY))
U=[flux/((ADOWN*teta)+BDOWN),((ADOWN*teta)+BDOWN)];
end;

if (teta >TETAXY)
U=[flux/LMIN,LMIN];
end;
```


APPENDIX V

```
% torque.m

% torque program (linear model)

% this program computes the output torque produced in one phase
% teta and current are the input variables

function T=f(TE);      % T is the output torque
                      % TE is the input line vector
E=TE';                % E is the input column vector
i=E(1);               % current %
teta=E(2);            % rotor position %

global TETAS TETAX TETAY TETAXY TETAON TETAOFF TETAQ V AUP BUP ADOWN BDOWN DL
LMIN LMAX

if ((0 <= teta) & (teta <= TETAX))
T=[0,0];              % torque is null since the inductance value, in this
                      % interval, is constant
end;

if ((TETAX < teta) & (teta <= TETAY))
T=[0.5*(DL)*(i*i),DL]; % torque signal obtained from equation (1.7)
end;

if ((TETAY < teta) & (teta <= TETAXY))
T=[-0.5*(DL)*(i*i),-DL];
end;

if (teta >TETAXY)
T=[0,0];
end;
```

APPENDIX VI

```

% int2.m

% initialization program (non-linear model)

% this program builds the look-up tables used in the SRM non-linear model

load sr.dat; X=sr; % load the numerical data obtained from fem analysis in [3]
couple=X(:,10); % the following commands rearrange the matrix data
M1=X(:,5); M2=X(:,6); X(:,12)=[]; X(:,11)=[]; X(:,9)=[]; X(:,8)=[]; X(:,7)=[];
%X(:,6)=[];
tet=X(:,1); cour=X(:,2); flu=X(:,3); angl=-45:0; angle=angl';

% Construction of the torque and mutual flux look-up tables
%
C=ones(21,46);
MU1=ones(21,46);
MU2=ones(21,46);
for i=1:21;
    for j=1:46;
        C(i,j)=couple(j+(i-1)*46);
        MU1(i,j)=M1(j+(i-1)*46);
        MU2(i,j)=M2(j+(i-1)*46);
    end;
end;

% Construction of the current look-up tables

A=zeros(21,46);
Bn=0:20;
for i=1:46;
    p=find(tet==(1-i));
    for j=1:21;
        A(j,i)=flu(p(j));
    end;
end;
fluxmax=A(21,1); don=0:fluxmax/1000:fluxmax; taille=size(don,2);
res=zeros(taille,46);

for i=1:46;
    x=A(:,i);
    xi=0:A(21,i)/200:A(21,i);
    y=0:20;
    yi=interp1(x,y,xi);
    for j=1:taille;
        gg=find(xi>=don(j));
        if gg==[]
            res(j,(47-i))=20;
        else
            res(j,(47-i))=yi(gg(1));
        end;
    end;
end;
end;

```

Fig. 1. Aligned position.

Fig. 2. Unaligned position.

Fig. 3: SRM linear model. Inductance profile of each phase.

Fig. 4. Angle δ corresponding to the displacement of a phase in relation to another.

Fig. 5. Matlab/Simulink diagram of the SRM linear model.

Fig. 6. Block *phase 1*.

Fig. 7. *H*-bridge asymmetric converter.

Fig. 8. Linear model: (a) phase inductance, (b) phase voltage, (c) phase current and (d) f.e.m.

Fig. 9. Linear model: (a) inductance, (b) voltage, (c) current, and (d) f.e.m.

Fig. 10. Linear model: (a) current in phase 1, (b) torque in phase1, (c) rotor speed, and (d) total torque.

Fig. 11. Linear model: (a) current in phase 1, (b) torque in phase 1, (c) rotor speed, and (d) total torque.

Fig. 12. Linear model: (a) current in phase 1, (b) torque in phase 1, (c) rotor speed, and (d) total torque.

Fig. 13. Linear model: (a) current and inductance, and (b) torque in phase 1.

Fig 14. Linear model: inefficiency of the current control by hysteresis for high speeds. Phase current.

Fig. 15. Inductance profile $L(\theta, I)$.

Fig. 16. Magnetic flux $\Psi(I, \theta)$

Fig. 17. Phase torque, $\Gamma(\theta, I)$.

Fig. 18. Non-linear SRM model: block *phase 1* without mutual inductances.

Fig. 19. Non-linear SRM model: (a) data of table flux/theta/current and (b) data of table current/theta/torque.

Fig. 20. Non-linear model and voltage control: (a) current, (b) torque, (c) speed, and (d) total torque.

Fig. 21. Non-linear model: (a) current in phase 1, (b) torque in phase 1, (c) speed, and (d) total

torque.

Fig. 22. Non-linear model: (a) current, (b) phase torque, (c) speed, and (d) total torque.

Fig. 23. Non-linear model: mean torque as function of I_{ref} and θ_{off} , $\Gamma_{mean} = g(I_{ref}, \theta_{off})$.

Fig. 24. Non-linear model: torque variance as function of I_{ref} and θ_{off} , $\sigma = f(I_{ref}, \theta_{off})$.

Fig. 25. Stator and rotor elements of the built 6/4 SR machine.

Fig. 26. H-bridge power converter.

Fig. 26. H-bridge power converter.

Fig. 27. Comparison of measured (a) and simulated (b) motor phase currents (Table I).

Fig. 28. Comparison of measured (a) and simulated (b) motor phase currents (Table I with $V_d = 100$ V).

Fig. 29. Comparison of measured (a) and simulated (b) motor phase currents using the voltage control method with the parameters listed in Table II.

Fig. 30. Steady-state performance. Measured and simulated motor speeds. (a) Results for $I_{ref} = 1.5$ A and (b) $I_{ref} = 2.5$ A using parameters listed in Table III.

TABLE I

OPERATING PARAMETERS OF SRM MODEL AND PROTOTYPE

$V_d = 150$ V	$I_{ref} = 2$ A	$\theta_{on} = 0^\circ$	$\theta_{off} = 22^\circ$
---------------	-----------------	-------------------------	---------------------------

TABLE II

OPERATING PARAMETERS OF SRM MODEL AND PROTOTYPE

$V_d = 30$ V	$I_{ref} = 2$ A	$\theta_{on} = 0^\circ$	$\theta_{off} = 30^\circ$
--------------	-----------------	-------------------------	---------------------------

TABLE III

OPERATING PARAMETERS OF SRM MODEL AND PROTOTYPE

$V_d = 150$ V	$\theta_{on} = 0^\circ$
---------------	-------------------------

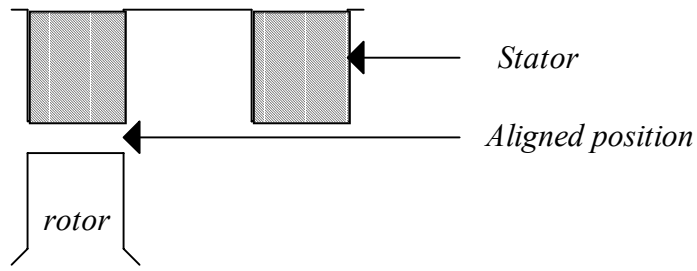


Fig. 1. Aligned position.

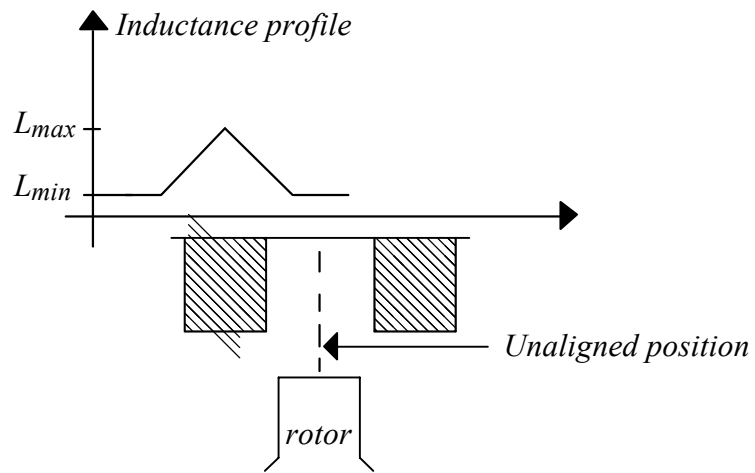


Fig. 2. Unaligned position.

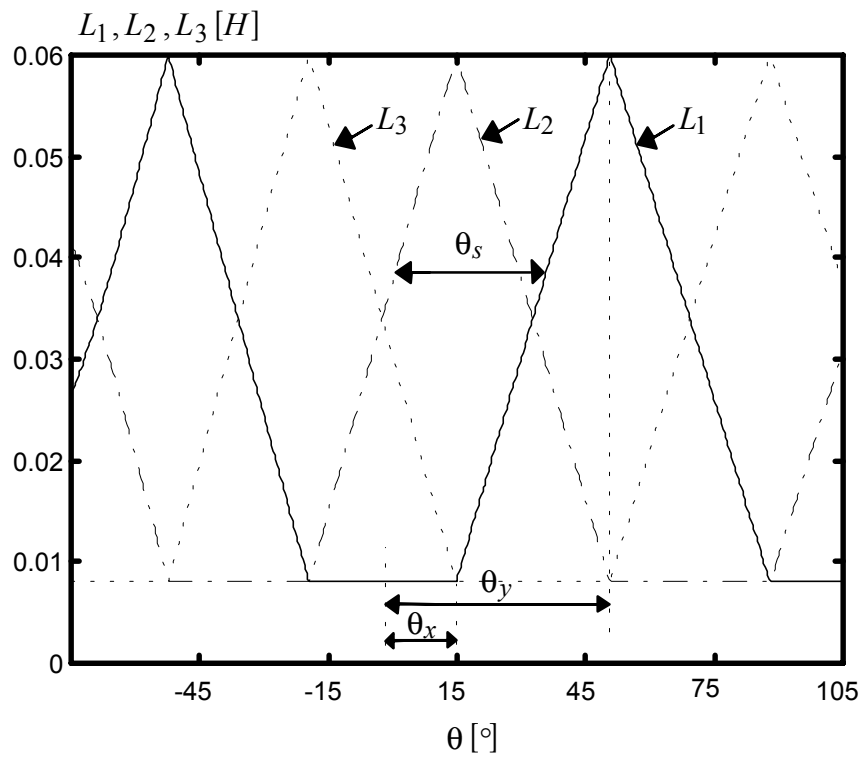


Fig. 3: SRM linear model. Inductance profile of each phase.

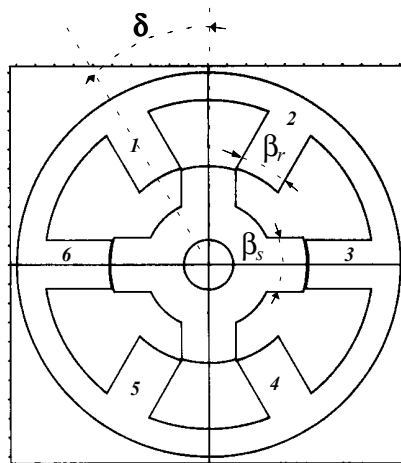


Fig. 4. Angle δ corresponding to the displacement of a phase in relation to another.

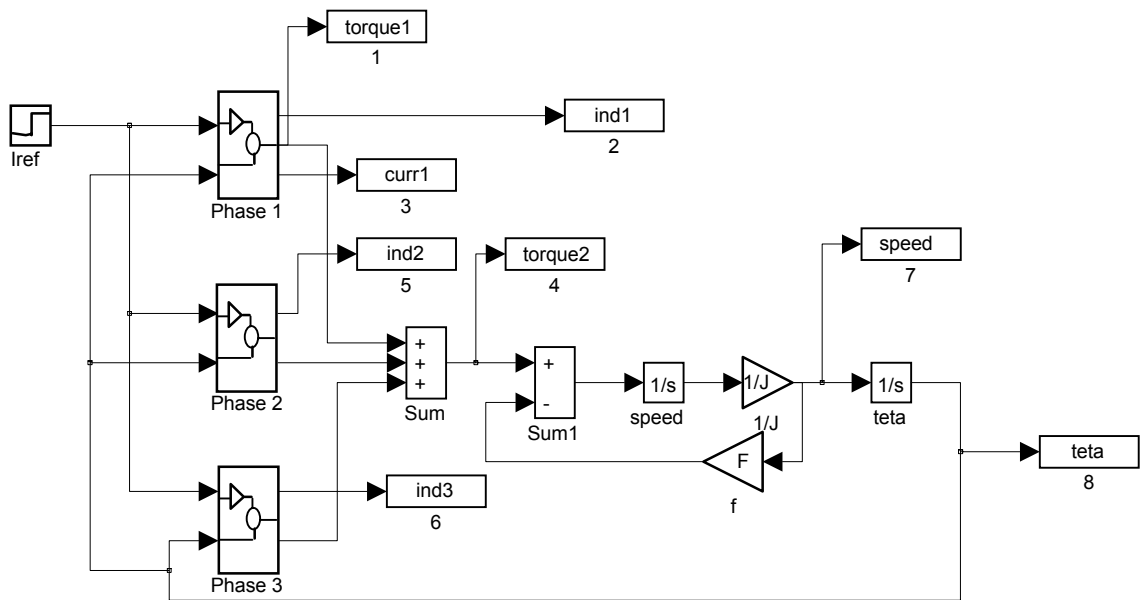
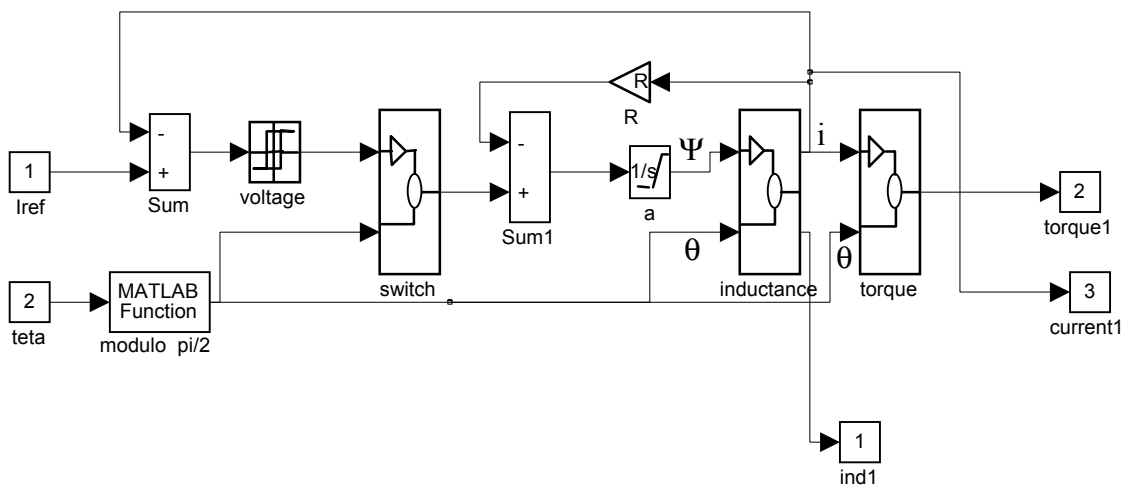


Fig. 5. Matlab/Simulink diagram of the SRM linear model.



Phase and converter models

Fig. 6. Block *phase 1*.

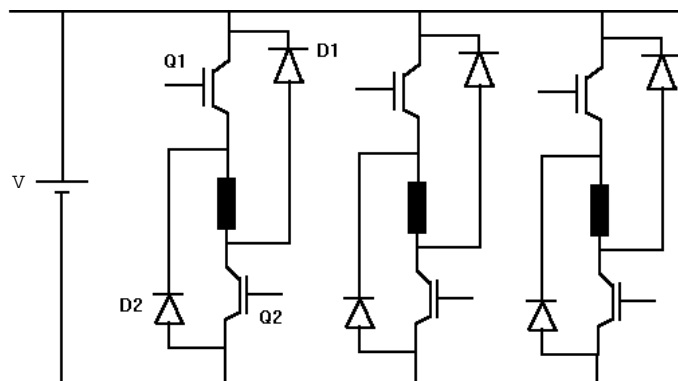
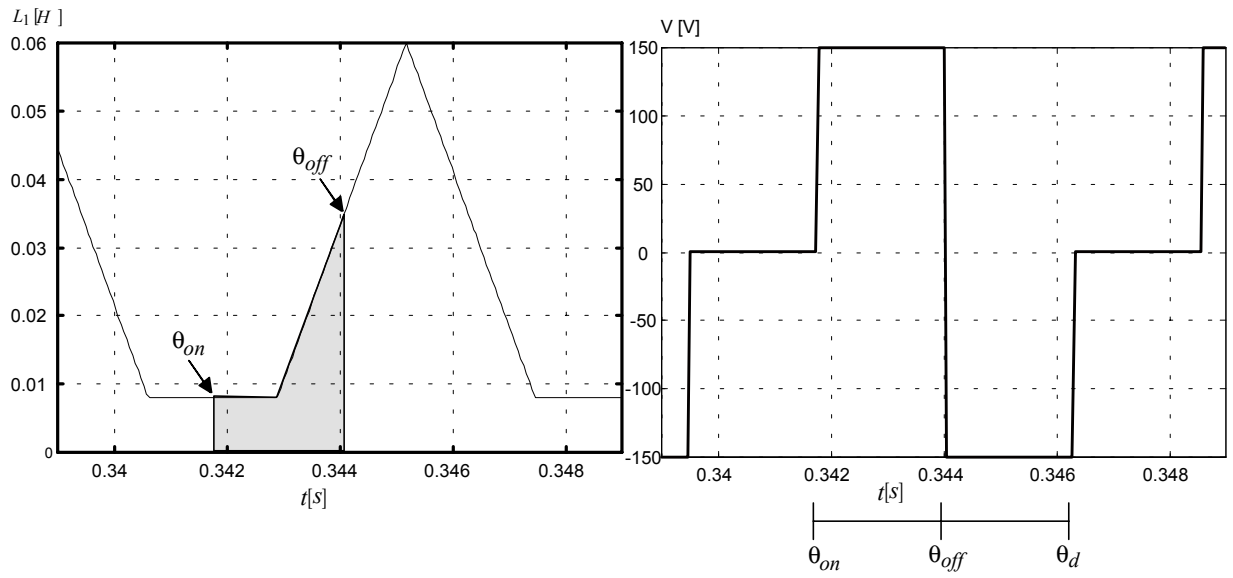
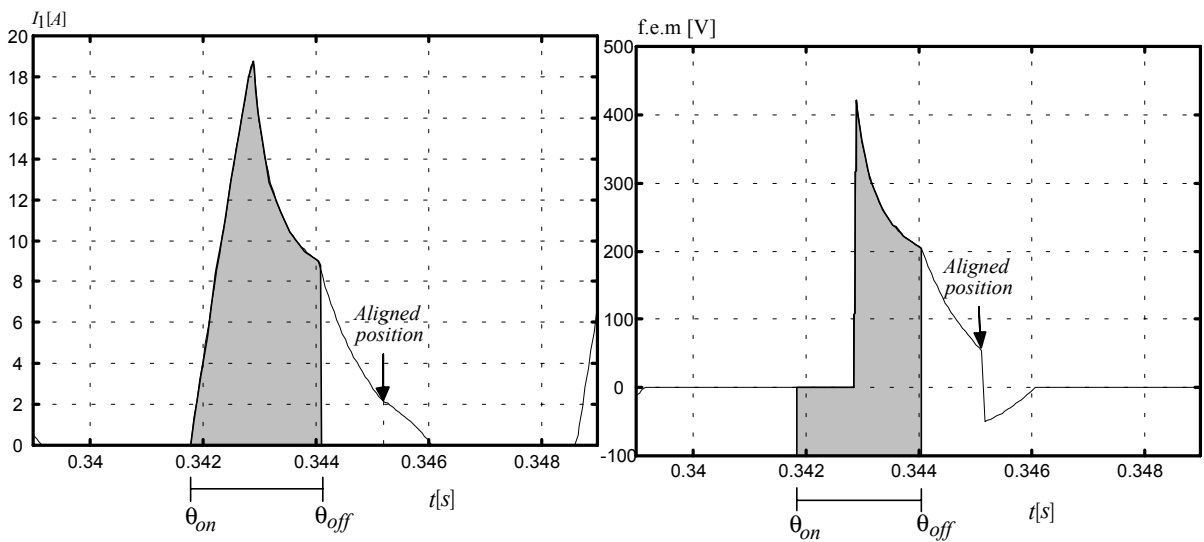


Fig. 7. *H*-bridge asymmetric converter.



(a)

(b)



(c)

(d)

Fig. 8. Linear model: (a) phase inductance, (b) phase voltage, (c) phase current and (d) f.e.m.

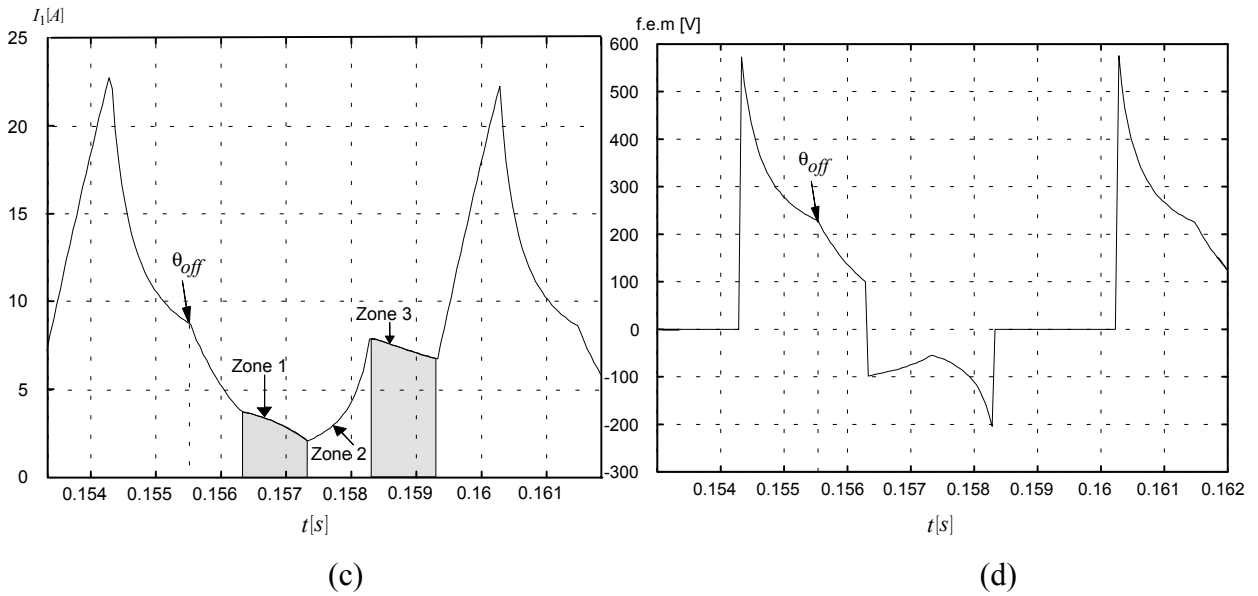
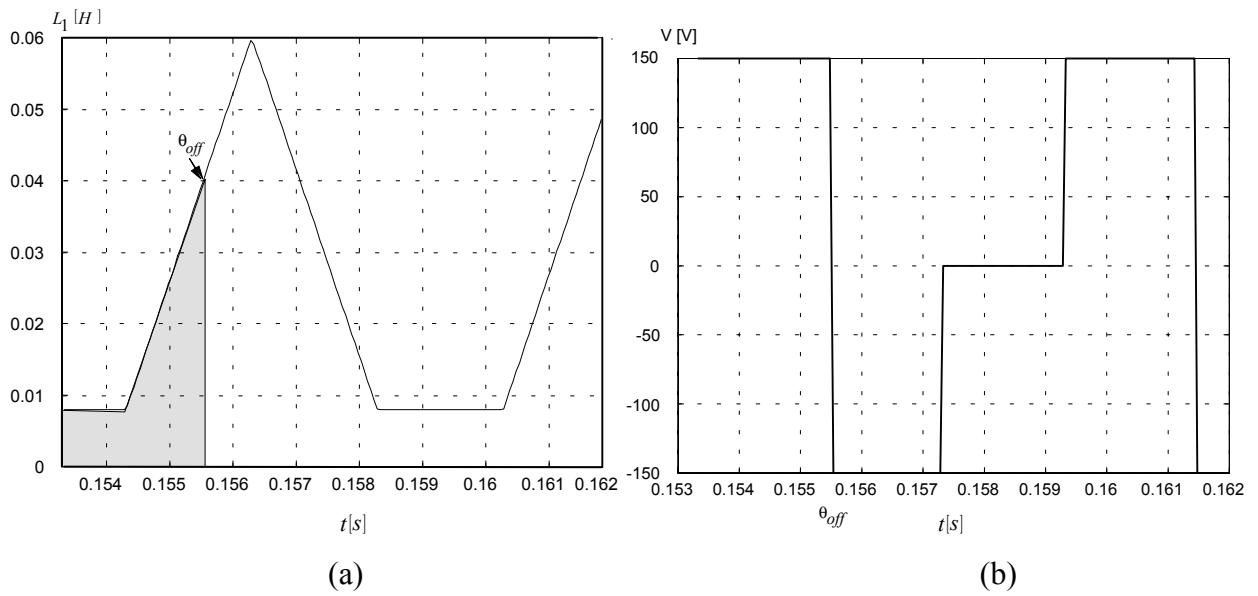
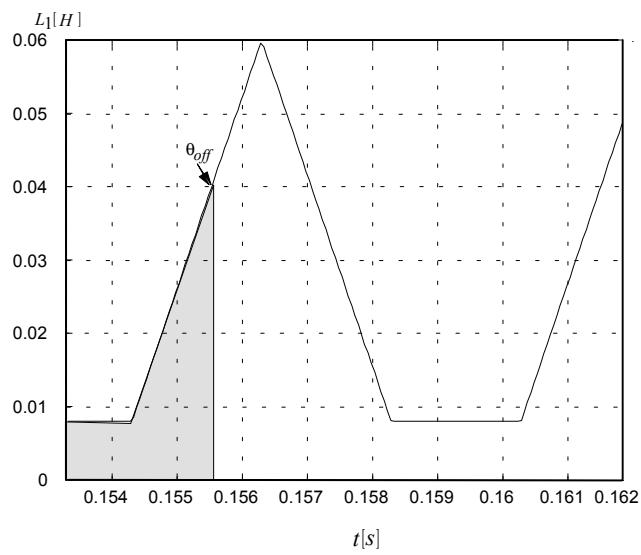
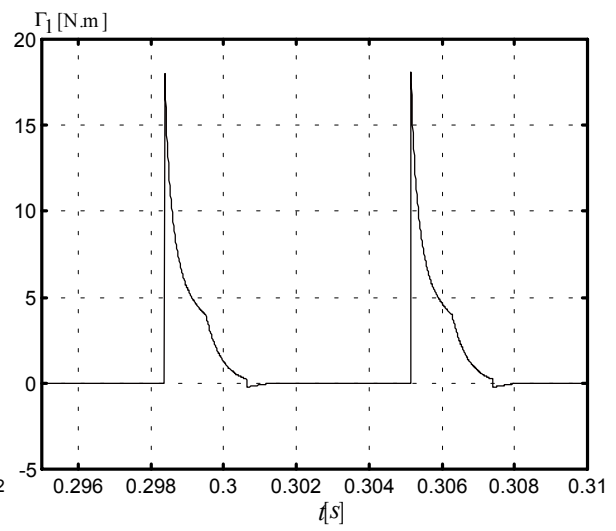


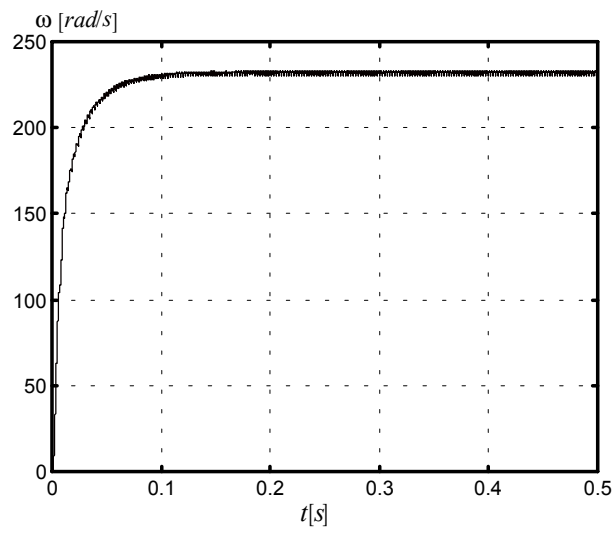
Fig. 9. Linear model: (a) inductance, (b) voltage, (c) current, and (d) f.e.m.



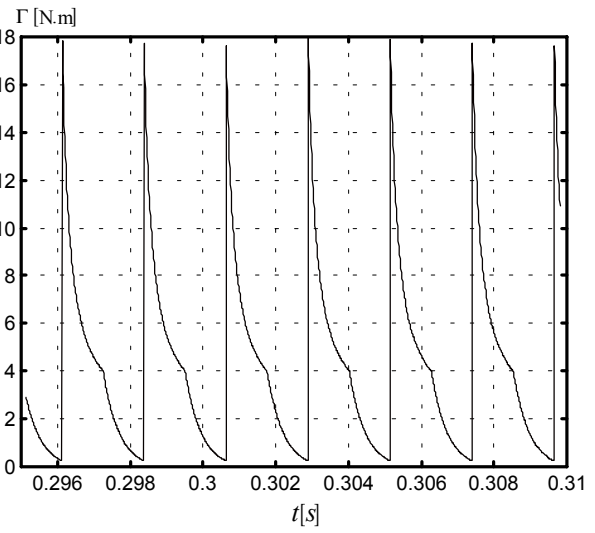
(a)



(b)



(c)



(d)

Fig. 10. Linear model: (a) current in phase 1, (b) torque in phase1, (c) rotor speed, and (d) total torque.

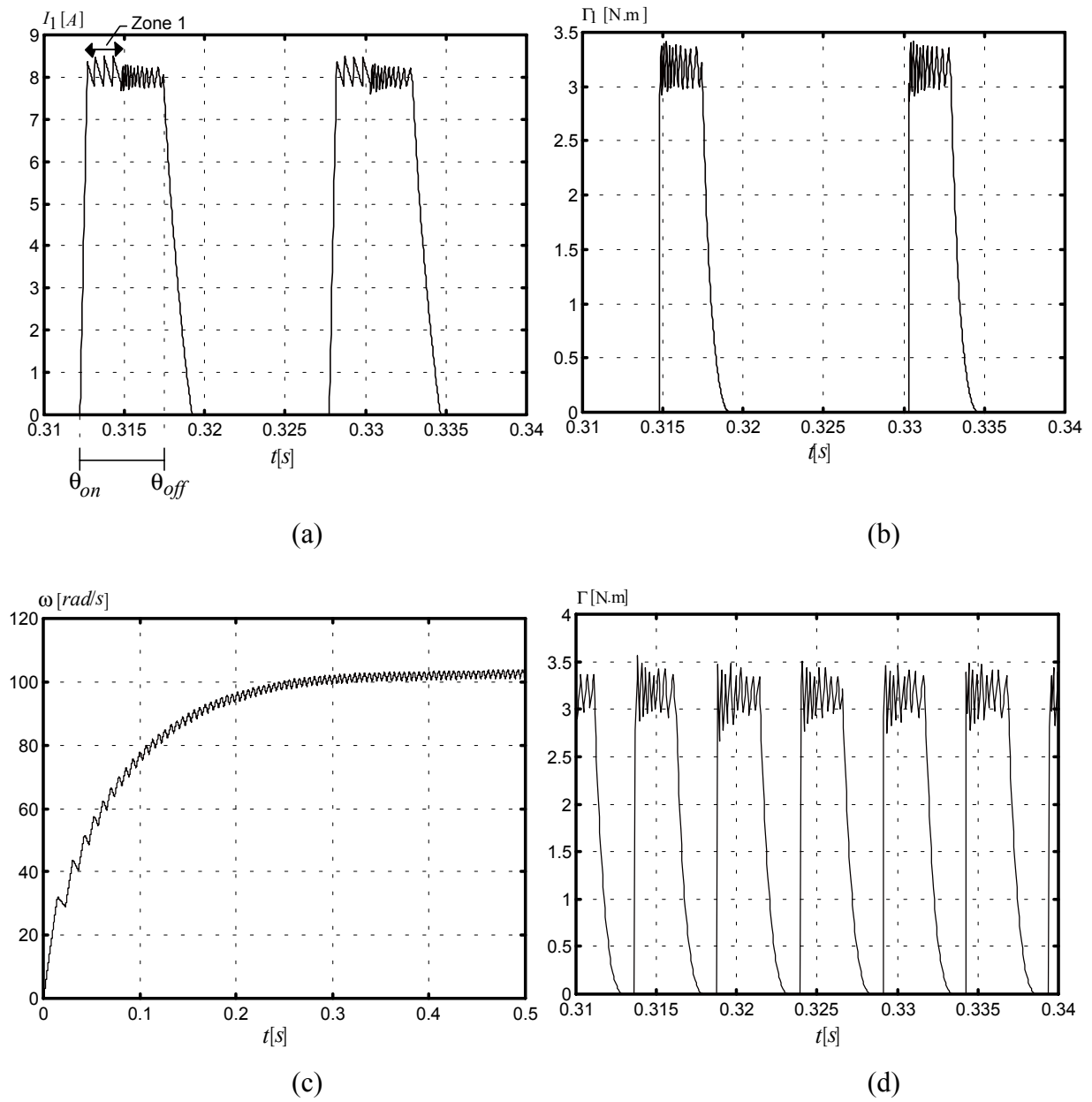


Fig. 11. Linear model: (a) current in phase 1, (b) torque in phase 1, (c) rotor speed, and (d) total torque.

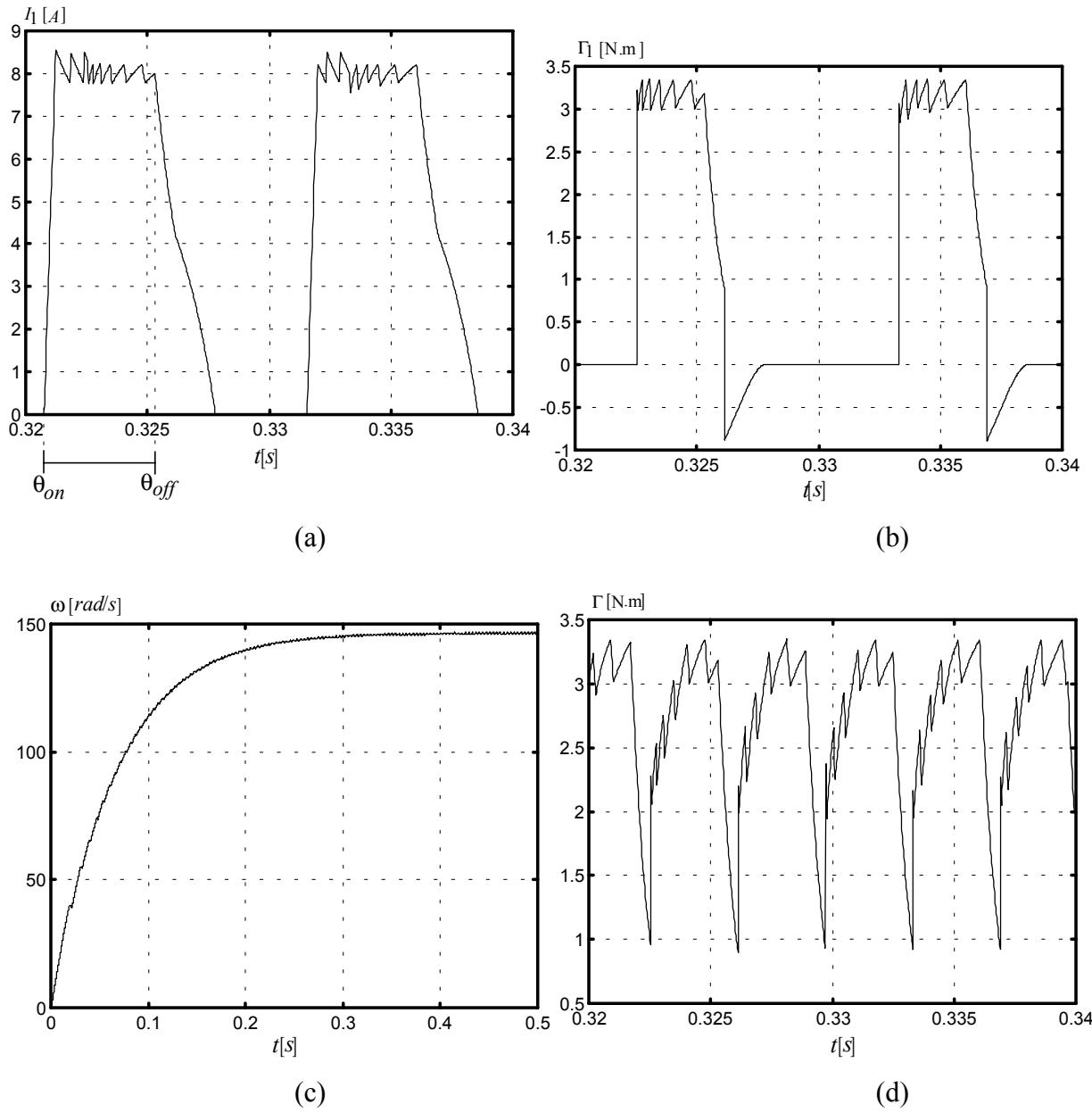


Fig. 12. Linear model: (a) current in phase 1, (b) torque in phase 1, (c) rotor speed, and (d) total torque.

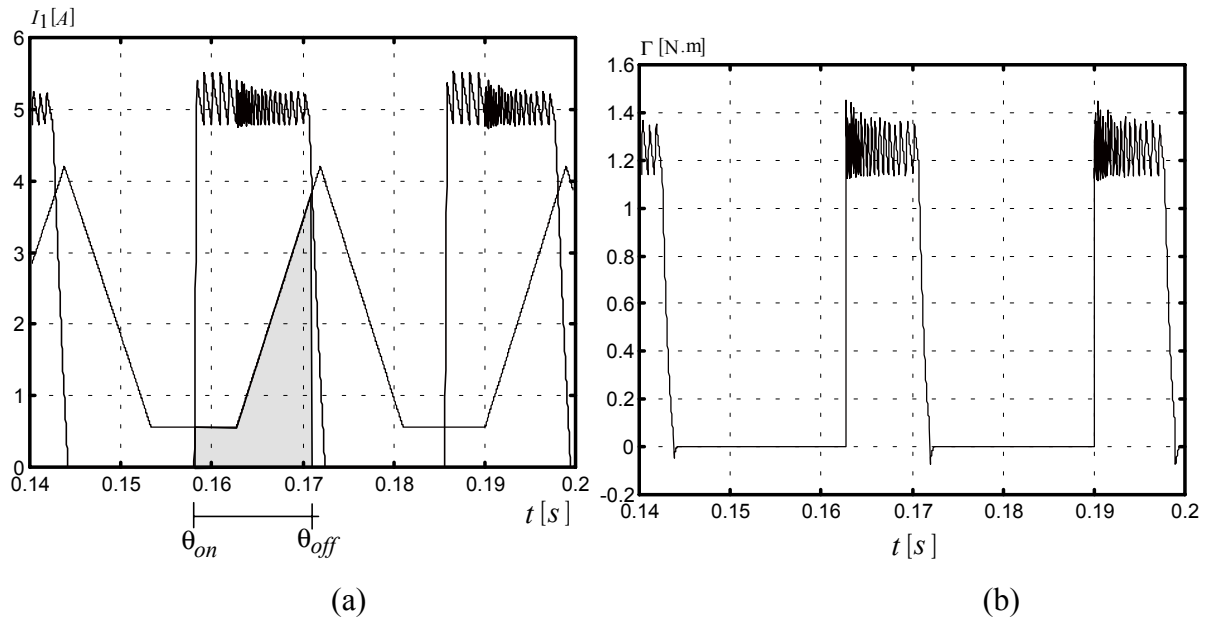


Fig. 13. Linear model: (a) current and inductance, and (b) torque in phase 1.

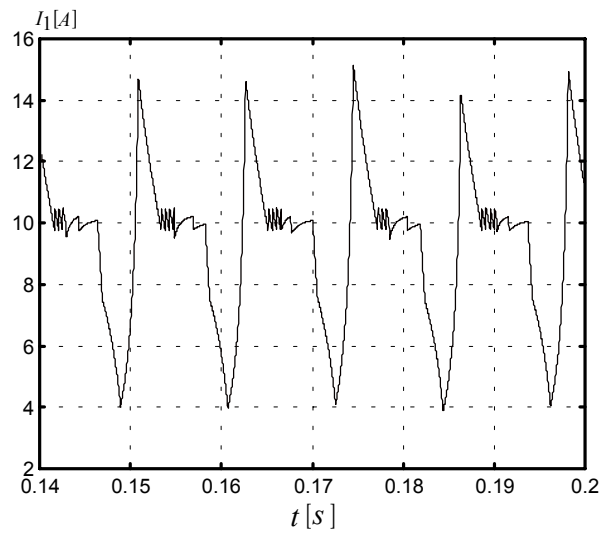


Fig 14. Linear model: inefficiency of the current control by hysteresis for high speeds. Phase current.

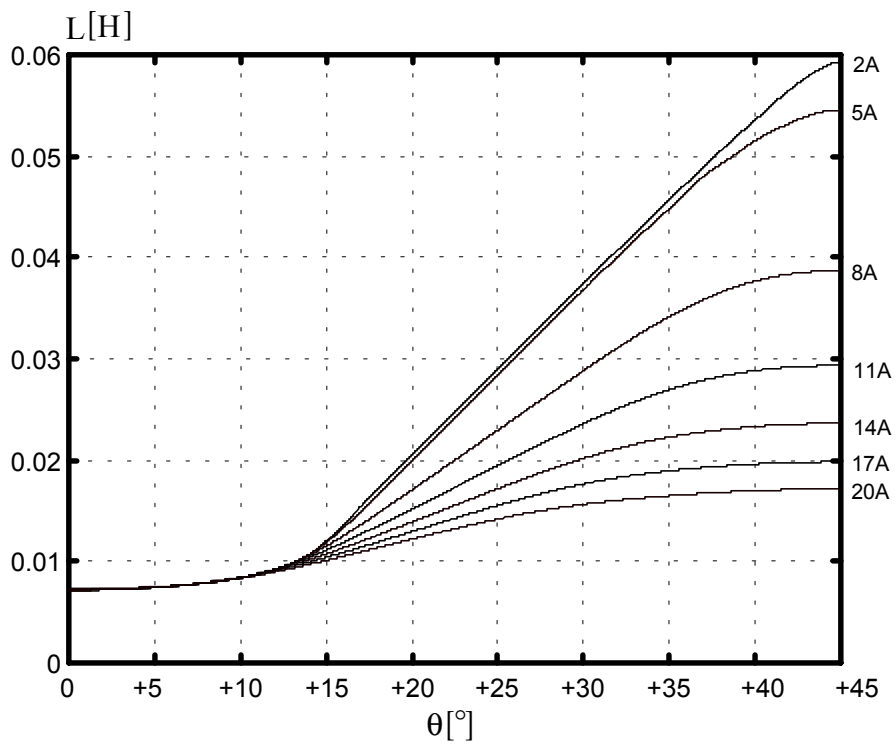


Fig. 15. Inductance profile $L(\theta, I)$.

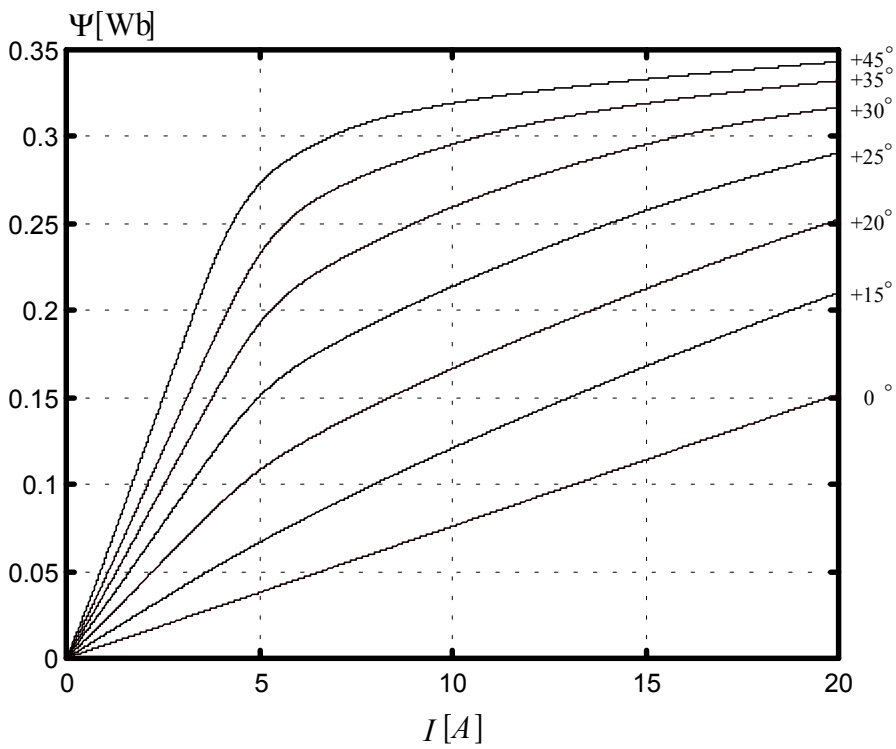


Fig. 16. Magnetic flux $\Psi(I, \theta)$

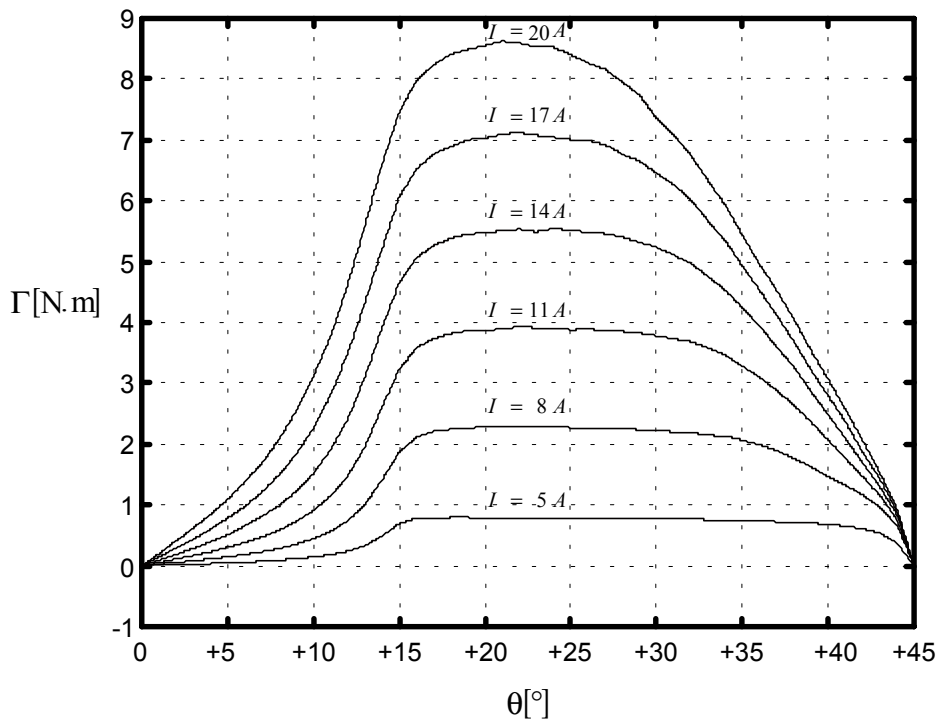


Fig. 17. Phase torque, $\Gamma(\theta, I)$.

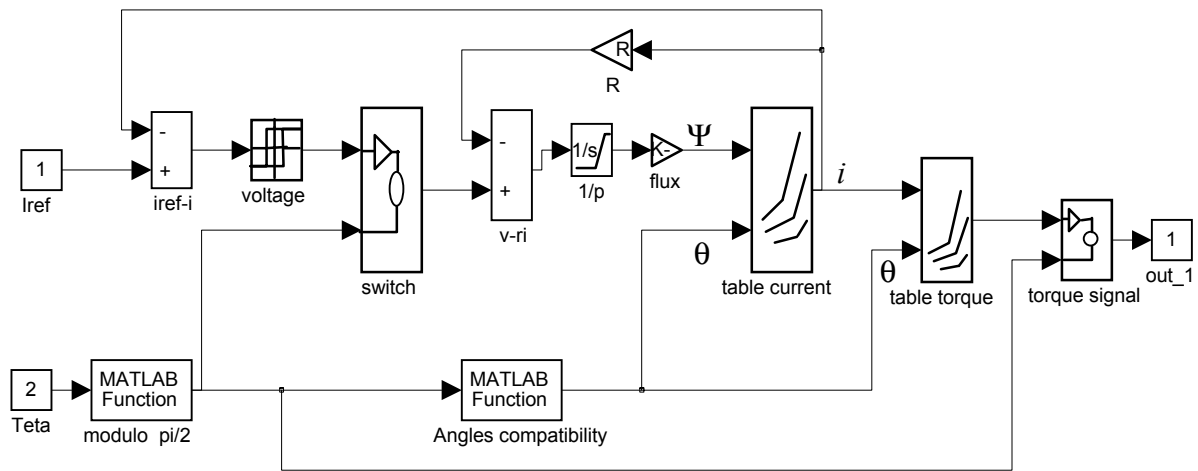
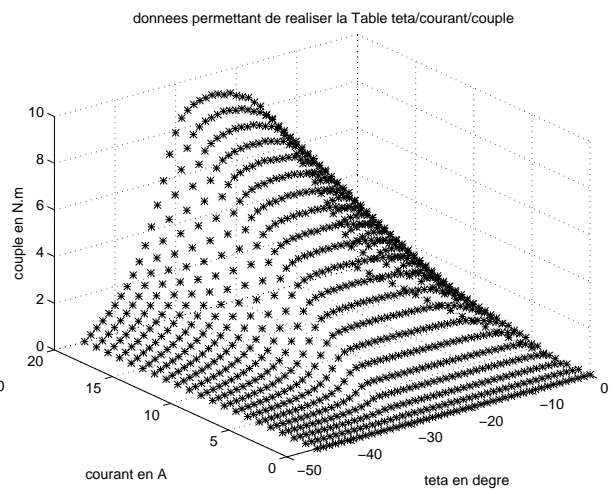
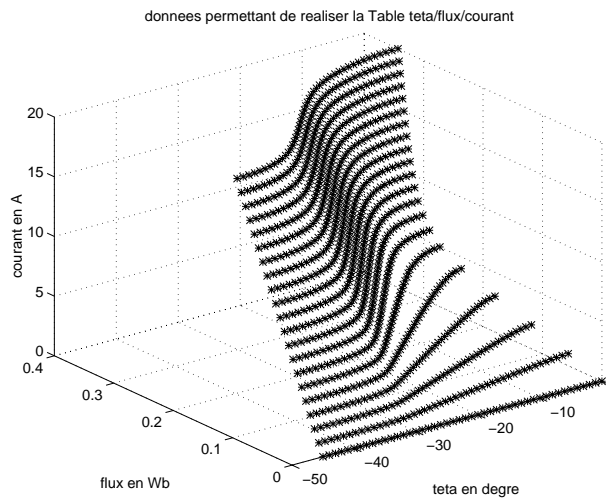


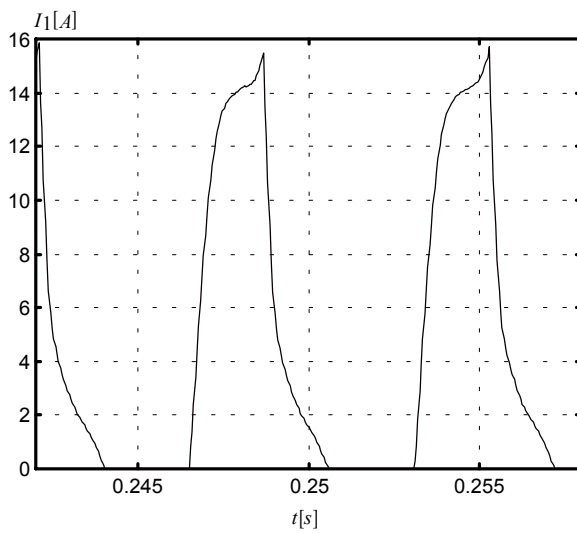
Fig. 18. Non-linear SRM model: block *phase 1* without mutual inductances.



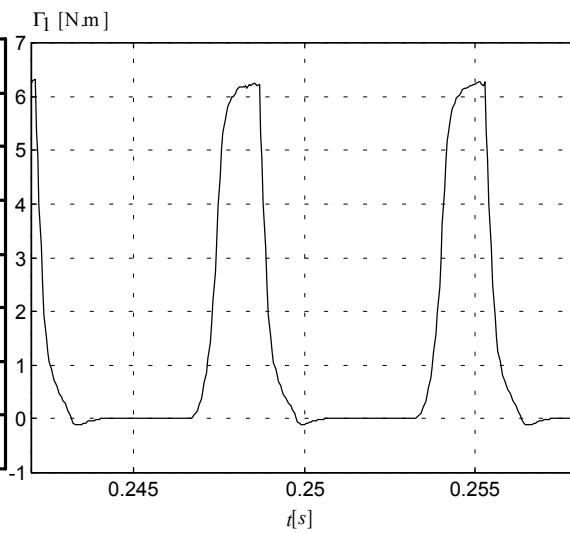
(a)

(b)

Fig. 19. Non-linear SRM model: (a) data of table flux/theta/current and (b) data of table current/theta/torque.



(a)



(b)

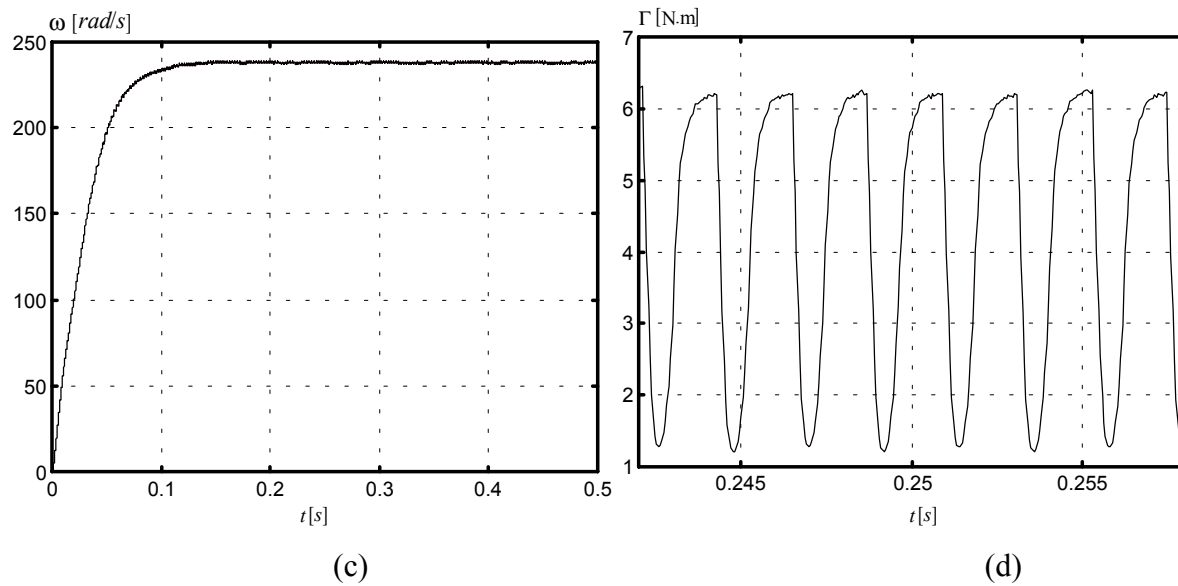


Fig. 20. Non-linear model and voltage control: (a) current, (b) torque, (c) speed, and (d) total torque.

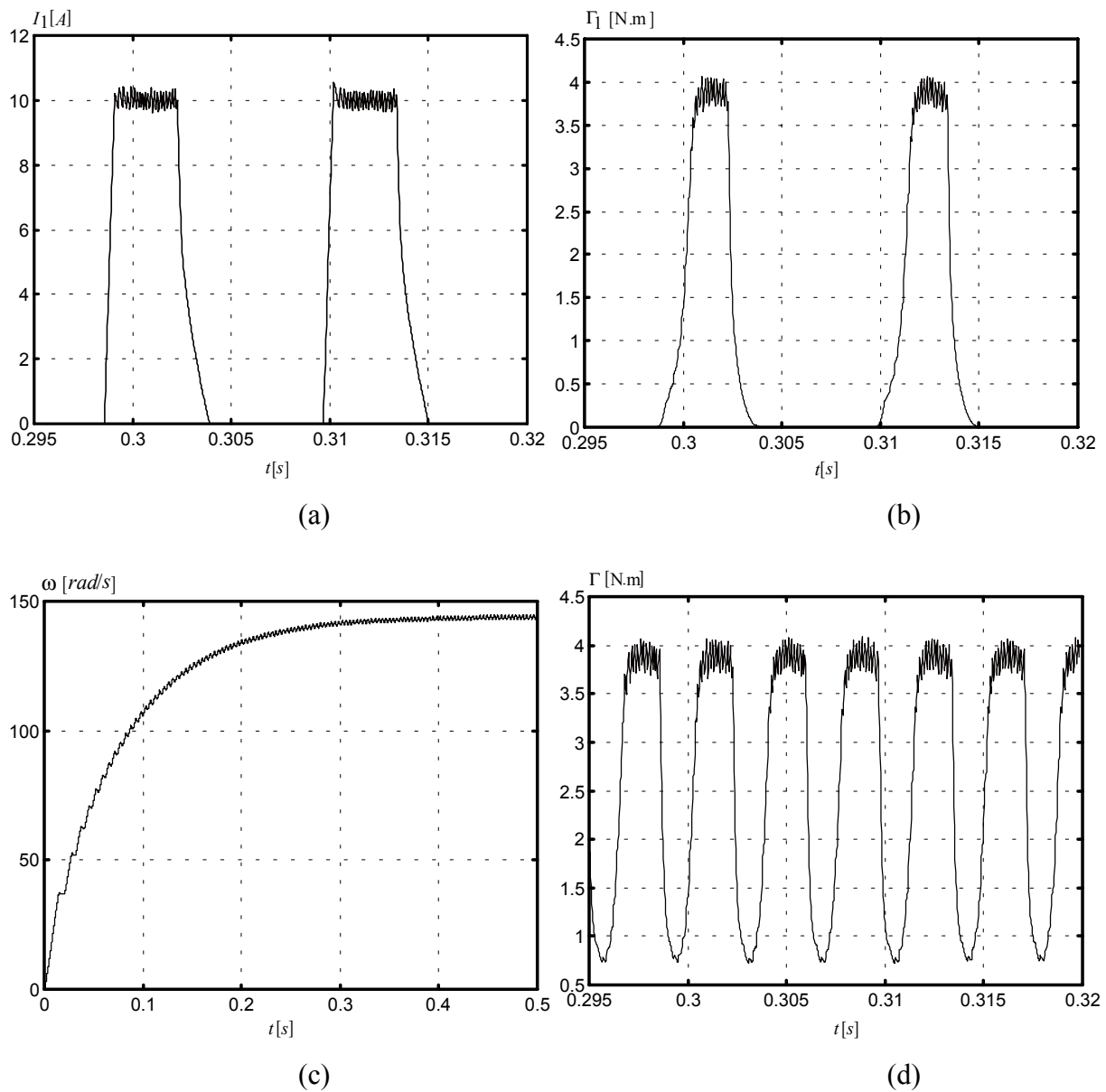
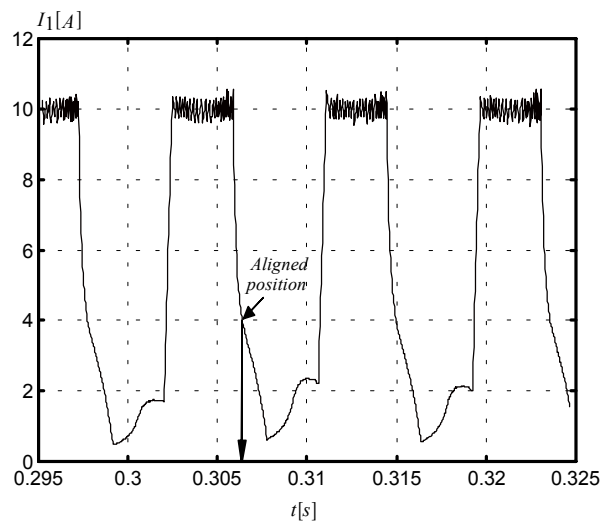
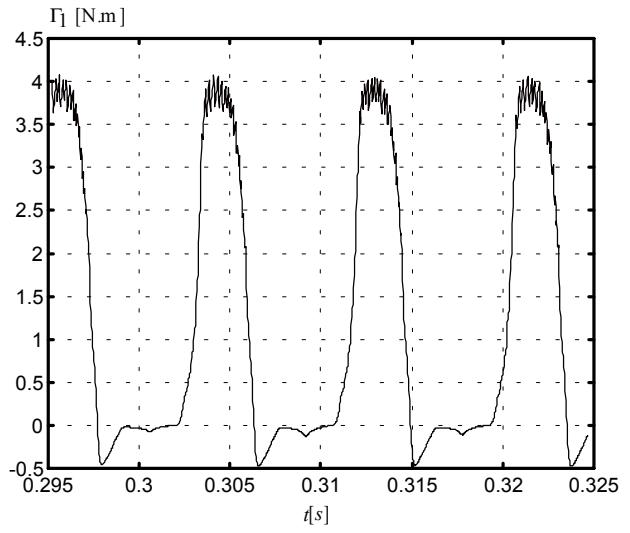


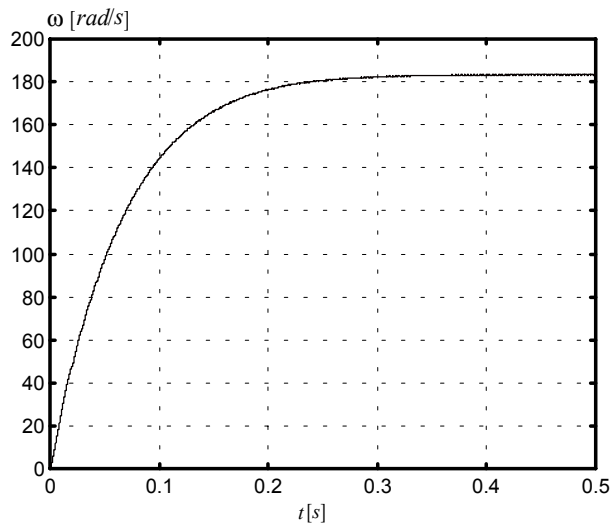
Fig. 21. Non-linear model: (a) current in phase 1, (b) torque in phase 1, (c) speed, and (d) total torque.



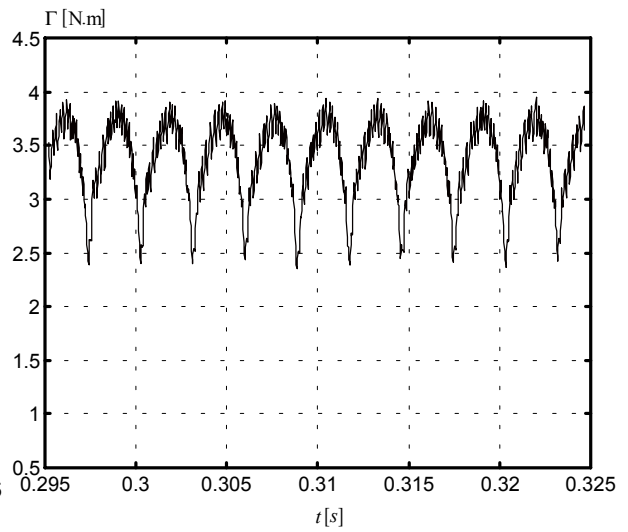
(a)



(b)



(c)



(d)

Fig. 22. Non-linear model: (a) current, (b) phase torque, (c) speed, and (d) total torque.

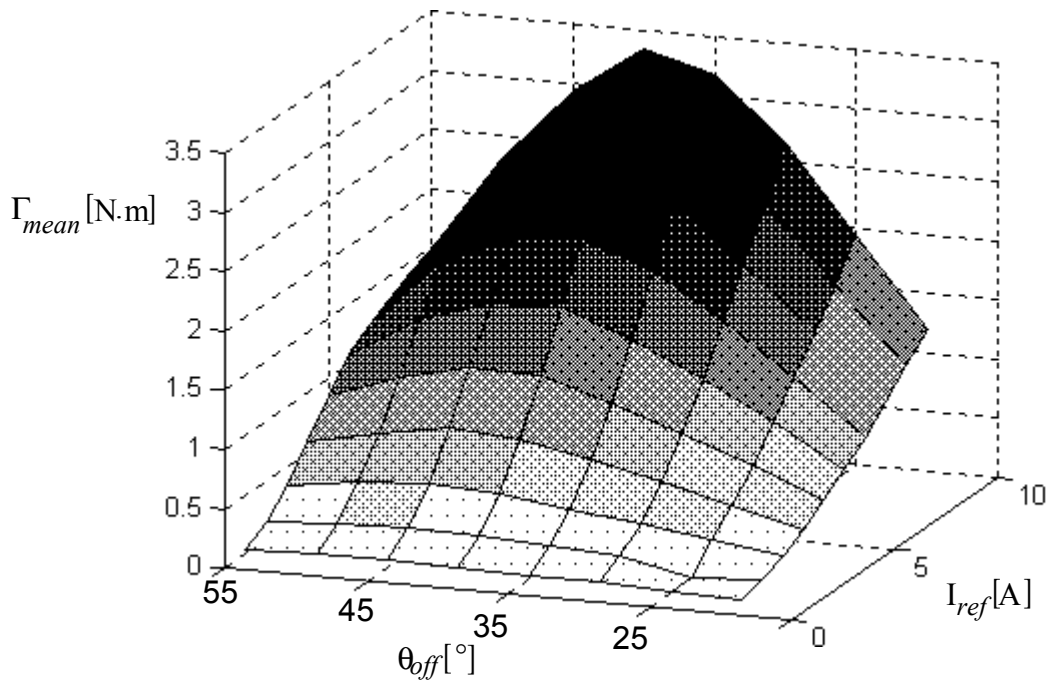


Fig. 23. Non-linear model: mean torque as function of I_{ref} and θ_{off} , $\Gamma_{mean} = g(I_{ref}, \theta_{off})$.

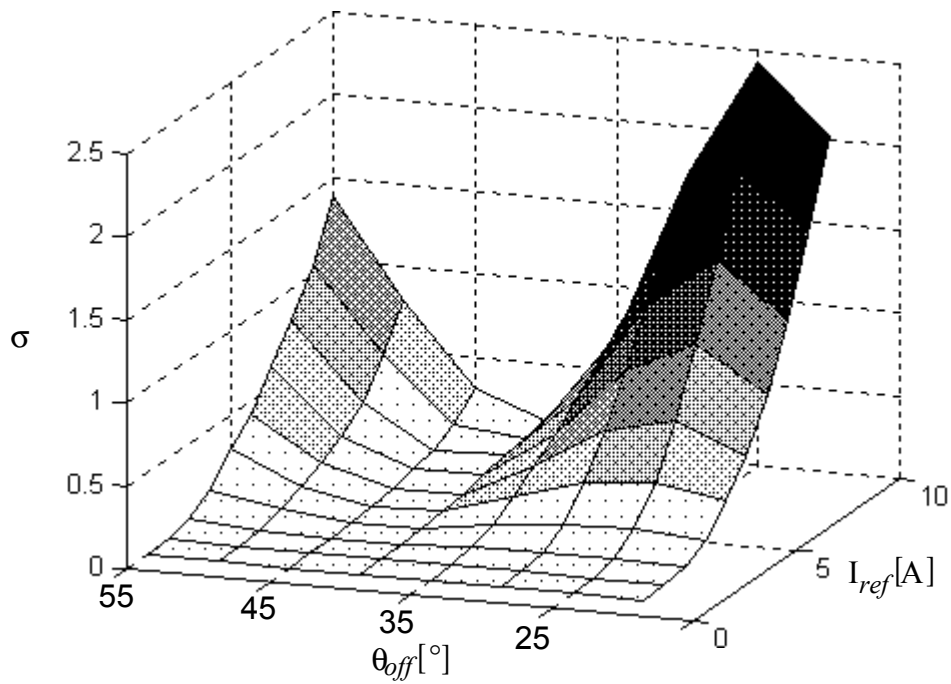


Fig. 24. Non-linear model: torque variance as function of I_{ref} and θ_{off} , $\sigma = f(I_{ref}, \theta_{off})$.

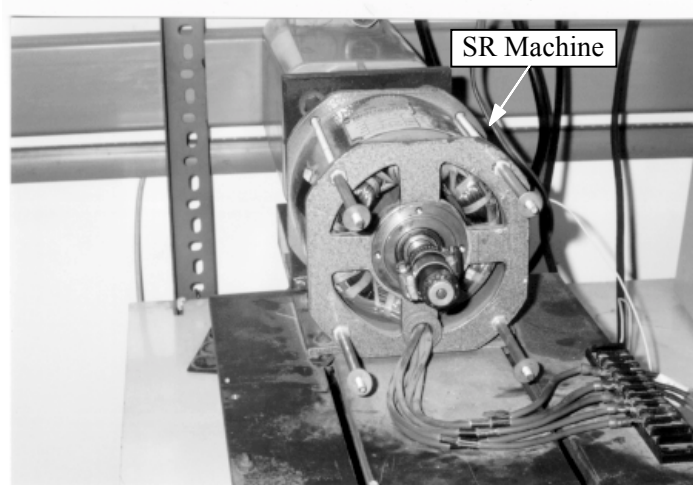


Fig. 25. Stator and rotor elements of the built 6/4 SR machine.

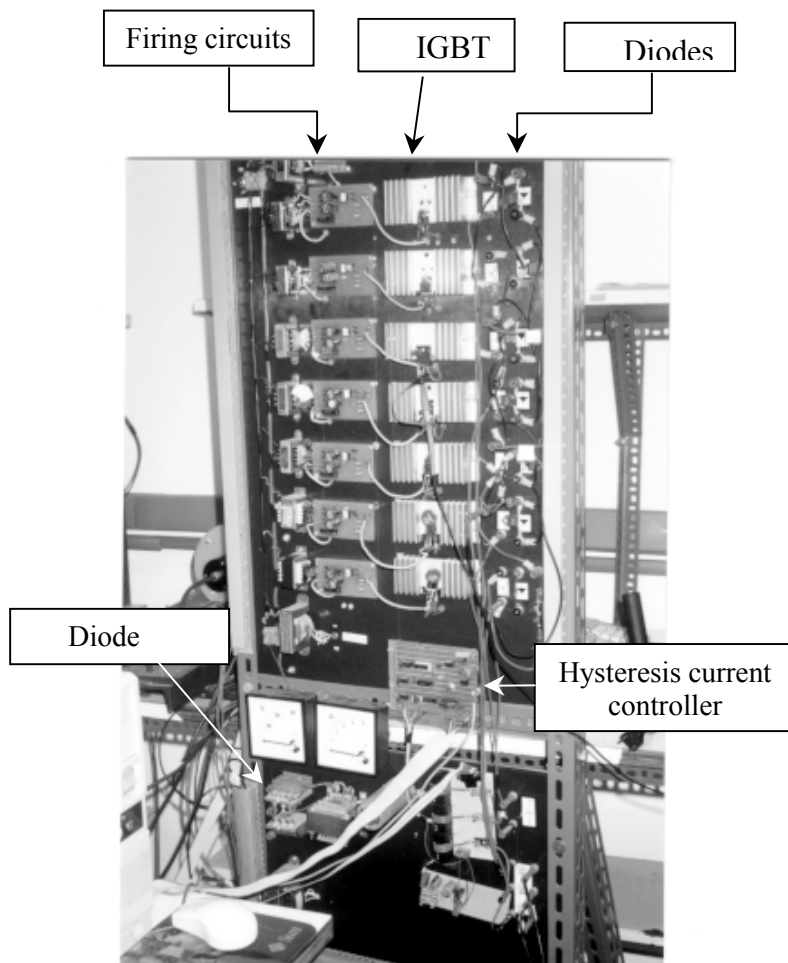
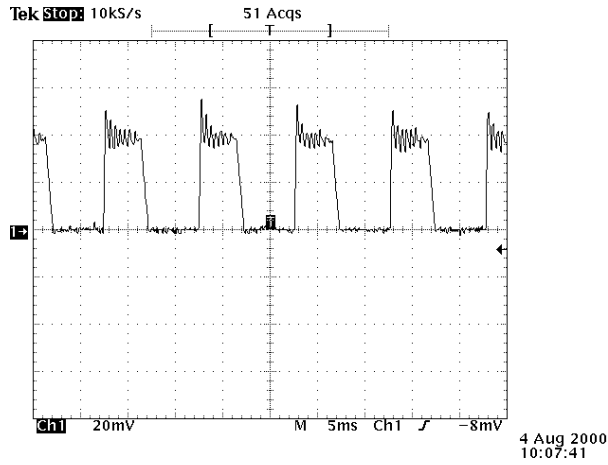
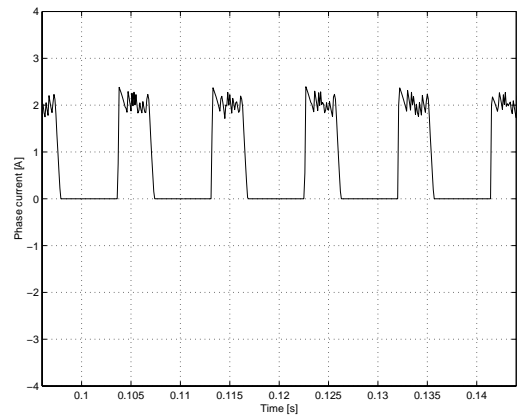


Fig. 26. H-bridge power converter.

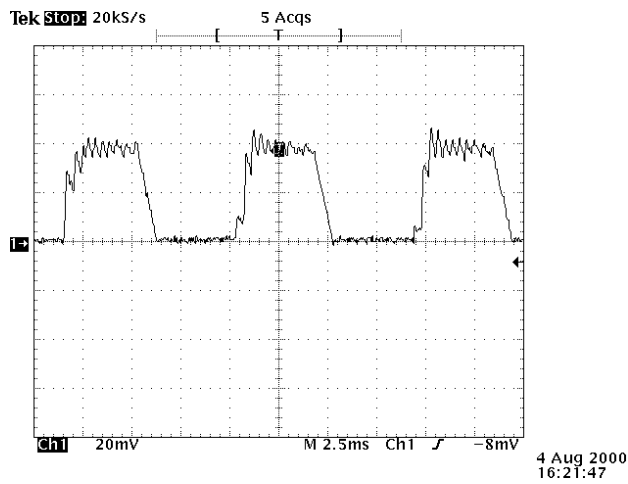


(a)

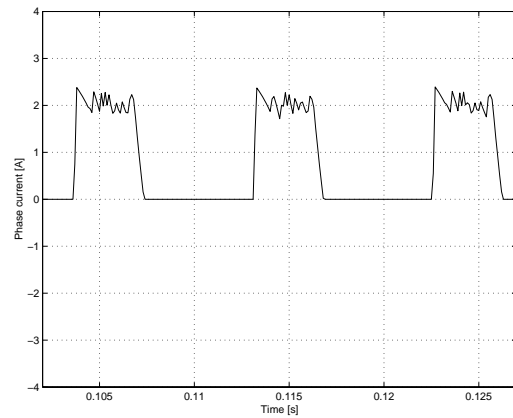


(b)

Fig. 27. Comparison of measured (a) and simulated (b) motor phase currents (Table I).

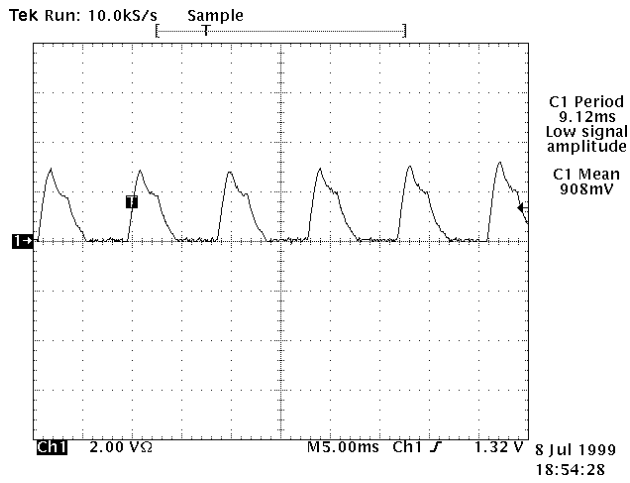


(a)

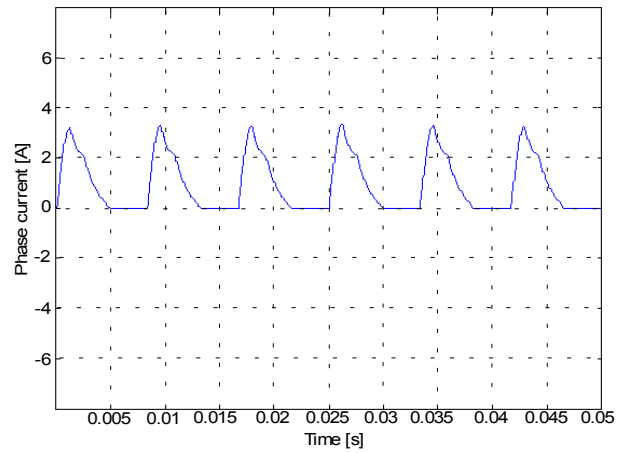


(b)

Fig. 28. Comparison of measured (a) and simulated (b) motor phase currents (Table I with $V_d = 100\text{ V}$).

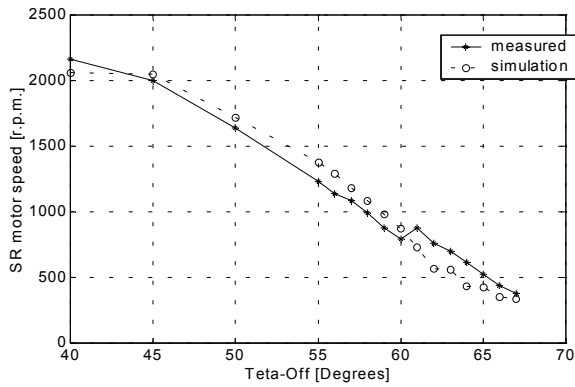


(a)

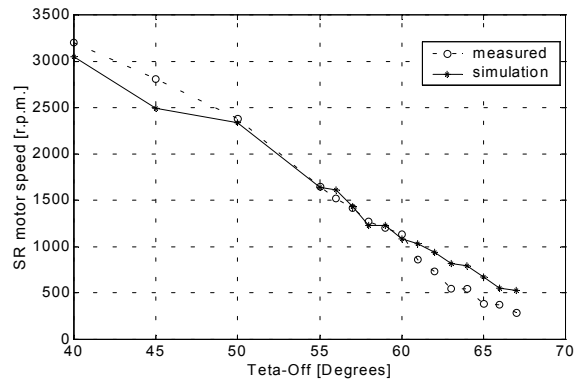


(b)

Fig. 29. Comparison of measured (a) and simulated (b) motor phase currents using the voltage control method with the parameters listed in Table II.



(a)



(b)

Fig. 30. Steady-state performance. Measured and simulated motor speeds. (a) Results for $I_{ref} = 1.5$ A and (b) $I_{ref} = 2.5$ A using parameters listed in Table III.